

Simulation Analysis of Cardiac Muscle Isotonic Contractions at Different Pre- and Afterloads

Natalie S. Schneider^{*,1,2} and Akira Amano²

¹Cell/Biodynamics Simulation Project Kyoto University, Japan; ²Department of Systems Science, Graduate School of Informatics, Kyoto University, Kyoto, Japan

Abstract: Since regulation of cardiac muscle contraction is complex, many simulation studies have been conducted to systematically analyze regulatory mechanisms underlying the force-velocity relationship. However, past studies were performed with models lacking detailed thin filament activation despite its essential regulatory role. Here a novel cardiac muscle contraction model is presented that considers troponin C, troponin I and tropomyosin for thin filament activation coupled with the cross-bridge (Xb) cycle, and in addition, includes a potential Frank-Starling mechanism and simple Xb mechanics. This model was employed to elucidate load and sarcomere length-dependence of the thin filament and Xb kinetics during muscle shortening and relaxation. Simulation analysis of afterloaded isotonic contractions performed at various preloads revealed that at medium to high load the peak Xb concentration, regulated by a load-dependent change of the ADP release rate, is the major factor in determining the end-systolic half sarcomere length, whereas the velocity-dependent Xb force only shows a small influence. At low load, shortening velocity is regulated through an increase in the rate of the tropomyosin conformational change as for all preloads the same Xb concentration is attained. Shortening-induced cooperative deactivation was caused by the included Frank-Starling mechanism. An analysis of newly suggested relaxation mechanisms showed the significance for an increased thin filament deactivation with troponin I pulling tropomyosin to the "off" position having a greater impact than titin restoring force assumed to disrupt the tropomyosin structure. A combination of this model with the myocyte Kyoto Model satisfactorily reproduced isotonic contraction time courses from guinea pig myocytes.

Keywords: Afterloaded isotonic contraction, muscle contraction modeling, force-velocity relationship, relaxation, titin, shortening-induced deactivation.

INTRODUCTION

Preload (PL) and afterload (AL), which are constantly changing in the intact heart, are important controllers of cardiac performance. In the heart the PL is indicated by the end-diastolic volume or pressure [1]. On the myocyte level the given PL establishes the maximum possible resting sarcomere length (SL), the SL from where contraction starts. This end-diastolic SL is the key in determining the active tension. As expressed in the length-tension relationship (LTR) the greater the initial SL, the higher the tension, which is the basis of the Frank-Starling law of the heart. The AL is the load sensed by the muscle after it starts to contract. For an efficient pump activity the heart has to adjust continually to the changing load. How load-dependent shortening and relaxation is regulated is still not completely understood. The force-velocity relationship (FVR) obtained from isotonic contractions, i.e., muscle shortening against a constant load, has been extensively studied for more than half a century by experiments [2-6] and simulations [6-10]. For a given PL with increasing AL velocity decreases in a hyperbolic manner. This is mainly the result of the interaction

between cross-bridge (Xb) mechanics and Xb kinetics known as mechano-chemical coupling.

Simulations with contraction models are a desirable method to determine potential rate limiting steps and regulatory mechanisms in the interaction between actin and myosin during shortening and relaxation due to an easy and systematic way to test rate parameter values. While many simulation studies which analyze the FVR have been published, the majority of the utilized models consider only the Xb cycle and neglect the thin filament and its activation state [8-10]. However, some models still include Ca^{2+} binding to troponin C (TnC) [11-13]. Since thin filament activation is an important part of muscle contraction, its influence cannot be ignored. In this study a cardiac muscle contraction model [14], which consists of separate steps for Ca^{2+} binding to TnC and the conformational changes of troponin I (TnI) and tropomyosin (Tm), in addition to the Xb cycle, was combined with simple Xb mechanics [11]. The model further includes a Frank-Starling mechanism and various mechanisms to express cooperativity in the activation of the thin filaments [14]. A major aim of this study was to use this, compared to other models, rather biological model for an analysis of regulatory mechanisms to advance the understanding in a field difficult to explore by experiments. Simulations of afterloaded isotonic contractions were performed in a quantitative way to analyze how different PLs and ALs affect thin fila-

*Address correspondence to this author at Department of Systems Science, Graduate School of Informatics, Kyoto University, Kyoto 606-8501, Japan; Tel.: 81-75-753-3375; Fax: 81-75-753-3375; E-mail: nati@biosim.med.kyoto-u.ac.jp

ment and Xb kinetics rate parameters and to determine the rate limiting step and its changes with load during shortening and relaxation. Furthermore, the effect of the Frank-Starling mechanism in isotonic contractions was analyzed. Potential relaxation mechanisms were tested.

Simulation results revealed that at medium to high loads the ADP release rate was the rate limiting step and determined the peak Xb concentration ([Xb]) which established the end-systolic SL, whereas at low load the Tm conformational change rate was rate limiting. Shortening-induced cooperative deactivation, for which so far a full mechanism is unaccounted for [15], could be explained by the inserted Frank-Starling mechanism. Moreover, relaxation velocity was more affected by the thin filament deactivation speed than a faster Xb detachment. Finally, the contraction model was designed to be easily combined with a myocyte model, as validated here using the Kyoto Model [16]. Its biological complexity allows for a precise change of rate parameters making the model suitable for future simulation studies of various pathophysiological conditions.

METHODS

Model Structure and Characteristics

In this study, a cardiac muscle contraction model previously used for an isometric contraction analysis [14], was extended for an analysis of isotonic contractions. This model shown in Fig. (1A) includes Ca²⁺ induced activation of the thin filaments and the Xb cycle and consists of seven states of a regulatory unit (RU), i.e., seven actin molecules, one Tm and one troponin (Tn) complex composed of TnC, TnI and TnT. RUA_MADPPi and RUA_MADP represent strong, i.e., force-generating, Xb states with both showing the same force. Instead, RUAMADPPi is a weak Xb state, which produces no force. Throughout the text a strong Xb is referred to as Xb and the sum of the two strong Xb states as [Xb]. Included in the model is a potential Frank-Starling mechanism as follows [14]: A SL-dependent change of the interfilament lattice spacing due to titin-based radial force modulates the [Xb] which affects the conformational change of TnI. A rise in the [Xb] results in a strong reduction of k_{offI}, the rate for the conformational change of TnI to the “off” state, and therefore prevents the back reaction. This mechanism provides a link between the strong [Xb] and the Ca²⁺ sensitivity of the thin filaments. Furthermore, it was assumed that only one myosin head can be bound per RU [14] as justified by calculations [17] stating that under fully activated isometric conditions only 0.37-0.75 myosin heads are bound per RU in the case that only one of both myosin heads of the molecule can be bound at the same time.

Mathematical Model

The complete set of equations for the model is given below. New mechanisms are described in detail while those previously explained [14] are briefly depicted. All parameters are defined in the glossary (APPENDIX). Constant parameter values are shown in Table 1.

Passive Tension

For a given PL the end-diastolic SL is determined by the passive tension (F_p). In the model the slack length (PL = 0)

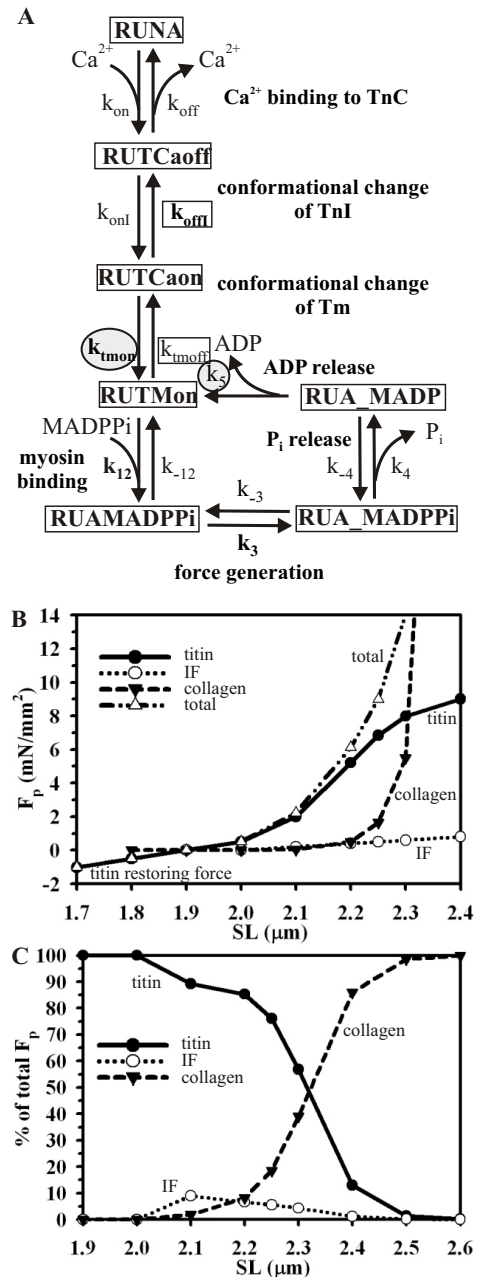


Fig. (1). Cardiac muscle contraction model. The state diagram for the model is shown in panel A. The model is composed of seven different states of a RU (RUNA: not activated RU; RUTCaoff: Ca²⁺ bound to TnC with TnI still bound to A; RUTCaon: TnI released from A; RUTMon: Tm in the activated conformation; RUAMADPPi: M with a hydrolyzed ATP bound to A of an activated RU = weak Xb; M pocket for P_i closed; RUA_MADPPi: strong Xb, M pocket for P_i open; RUA_MADP: strong Xb, P_i released from the acto-myosin complex). The bold rate parameters k_{offI}, k_{tmon} and k₃ are changing due to cooperativity. k₁₂ depends on titin-based radial force. The rate parameters indicated by a circle (k_{tmon}, k₅) are load-dependent. The boxed rate parameters (k_{tmoft}, k_{offI}) are subject to changes during relaxation. Panel B depicts the SL-dependent changes of F_p. Panel C shows how much each contributor effects F_p at a given SL above slack length.

was set to 1.9 μm in accordance to experimental data from guinea pig cardiomyocytes [18]. F_p was split into three parts, one for each molecular contributor, namely titin and the intermediate filaments, which are intracellular contributors, and collagen with an extracellular action (Fig. 1B). The degree of contribution to F_p was fit to experimental data from rat trabeculae [19] (Fig. 1C). Titin accounts for over 70% of F_p from slack length to 2.25 μm . This percentage drops to below 20% at 2.4 μm . Intermediate filaments contribute 10% from slack length to 2.1 μm , which decreases to 3% at 2.3 μm . Collagen prevents the sarcomere from overstretching while playing a minor role at the physiological SL range. Collagen contribution rises slowly from 0% at 2 μm to about

20% at 2.25 μm , but reaches over 80% at about 2.4 μm . Titin-based restoring force is responsible for F_p below slack length [20,21], but so far could not be quantitatively measured. A linear equation was chosen to describe the half SL- F_p relation for intermediate filaments (F_{pIF}).

$$\text{For } L > 0.001 \text{ mm: } F_{pIF} = 4.0(L/L_0) - 4.0 \quad (1)$$

$$\text{For } L \leq 0.001 \text{ mm: } F_{pIF} = 0$$

with L the half SL and L_0 a normalization factor. All F_p fractions are given in mN/mm^2 .

The data for collagen-based F_p (F_{pEx}) were fitted to an exponential function:

Table 1. Numerical Values of Parameters

Parameter	Value	Source
A_f	$1.1 \times 10^9 \text{ mN}/\text{mm}^3/\text{mM}$	Model fit
k_{off}	0.2 /ms	[62]
k_{on}	17.3 /mM/ms	[62]
[RUtotal]	0.0726 mM	Calculated for $L_{max}=1.1\mu\text{m}$ according to [17]
k_{onI}	0.11 /ms	Model fit
k_{offI}	0.055 /ms	Model fit
k_{OFF}	-0.265	Model fit
k_{xboff}	-1.37	Model fit
k_{tmoff}	0.067 /ms	Model fit [63]
k_{tmoc}	0.014 /ms	Model fit [63]
k_{tmRU}	10	Model fit
k_{tmxb}	-1.86	Model fit
$k_{offrelax}$	20	Model fit
L_0	0.001 mm	to normalize L
k_{12}	2 /mM/ms	Model fit according to [9,64]
k_{-12}	0.6 /ms	Model fit according to [9,64]
[MADPPi]	0.1375 mM	Calculated for $L_{max}=1.1\mu\text{m}$ according to [17]
k_{Titin}	0.2	Model fit
k_{3c}	0.025 /ms	Model fit according to [64]
k_{3f}	50	Model fit
k_{3xb}	-1.23	Model fit
k_{-3}	0.008 /ms	Model fit according to [64]
k_4	0.077 /ms	[45]
k_{-4}	0.001 /ms	Model fit
k_5 (for load fraction =1)	PL 0: 0.05439 /ms PL 0.51: 0.0546543 /ms PL 2.25: 0.0372306 /ms	Model fit (constant for isometric contractions)
h_c	3.6 nm for 5°C 5.0 nm for 17°C 6.1 nm for 37°C	Fit to experimental data [24]
K_p	0.0002 mM/ms	Model fit
Q_m	0.00095 mM/ms	Model fit
K_m	0.0001 mM	[11]
t_1	25 ms	[11]

$$\text{For } L \geq 0.001 \text{ mm: } F_{pEx} = 0.20/47.84 \times \left(e^{47.84 \cdot (L/L_0)^{-1}} - 1 \right) \quad (2)$$

$$\text{For } L < 0.001 \text{ mm: } F_{pEx} = 0$$

Titin-based F_p (F_{pTitin}) was separated into passive tension measured above slack length and titin's restoring force below slack length:

For $L < 0.001$ mm:

$$F_{pTitin} = \frac{9.3323}{0.05/0.95 \times \left(1 + e^{(1.0924-1)/0.0324} \right)} \cdot \left(L/(L_0 \times 0.95) - 1 \right) \quad (3)$$

$$\text{For } L \geq 0.001 \text{ mm: } F_{pTitin} = \frac{9.3323}{1 + e^{((-L/L_0)+1.0924)/0.0324}}$$

$$\text{The total } F_p \text{ is given by: } F_p = F_{pIF} + F_{pTitin} + F_{pEx} \quad (4)$$

Cross-bridge Kinetics

The sum of all RUs (RU_{total}) is given by: (5)

$$[RU_{total}] = [RUNA] + [RUTCaoff] + [RUTCaon] + [RUTMon] + [RUAMADPPi] + [RUA_MADPPi] + [RUA_MADP]$$

The net rate of Ca^{2+} binding to TnC (Q_{CaB}) is calculated as follows:

$$Q_{CaB} = k_{on} [RUNA] [Ca^{2+}] - k_{off} [RUTCaoff] \quad (6)$$

The net rate for the conformational change of TnI (Q_{TCA}) is expressed as:

$$Q_{TCA} = k_{onI} [RUTCaoff] - k_{offI} \times k_{relaxTnI} [RUTCaon] \quad (7)$$

The rate parameter for the change of TnI to the "off" conformation (k_{offI}) changes due to positive cooperativity caused by neighboring activated RUs (RUA) (first term) and strong Xbs (second term): (8)

$$k_{offI} = k_{offI} \left[1 + k_{OFF} \left(\frac{[RUA]}{[RU_{total}]} \right) \right]^2 \times \left[1 + k_{xbOff} \left(\frac{[RUA_MADPPi] + [RUA_MADP]}{[RU_{total}]} \right) \right]^{4.4}$$

with

$$[RUA] = [RUTCaon] + [RUTMon] + [RUAMADPPi] + [RUA_MADPPi] + [RUA_MADP] \quad (9)$$

The factor $k_{relaxTnI}$ enhances relaxation at low load (see section "Relaxation Mechanisms").

The net rate for the conformational change of Tm (Q_{TMA}) is given by:

$$Q_{TMA} = k_{mon} \times k_{loadTM} [RUTCaon] - k_{moff} \times titinRF \times k_{offTnI} [RUTMon] \quad (10)$$

The Tm conformational change rate to the "on" state given by k_{mon} is subject to positive cooperativity due to activated RUs (first and second term in Eq. 11) and negative cooperativity due to strain caused by strong Xbs (third term): (11)

$$k_{mon} = k_{monc} \left(\frac{[RUTCaon]}{[RU_{total}]} \right) \times \left[1 + k_{mRU} \left(\frac{[RUTMon]}{[RU_{total}]} \right) \right]^2 \times \left[1 + k_{mb} \frac{([RUA_MADPPi] + [RUA_MADP])^2}{[RU_{total}]} \right]$$

The factor k_{loadTM} enhances the Tm conformational change at low load shortening (see section "Simulations of Afterloaded Isotonic Contractions"). The factors $titinRF$ and k_{offTnI} speed up relaxation (see section "Relaxation Mechanisms").

The net rate of the myosin binding step (Q_{MB}) resulting in the formation of weak Xbs is calculated as follows:

$$Q_{MB} = k_{12} \times KTitin [MADPPi] \times [RUTMon]_{eff} - k_{-12} [RUAMADPPi] \quad (12)$$

The fraction of activated RUs overlapping with the myosin filaments called effective fraction is given by:

$$[RUTMon]_{eff} = \alpha [RUTMon] \quad (13)$$

The sarcomere overlap function α describes the SL-dependent change of the myosin filament fraction which overlaps with the actin filament:

$$\text{For } L < 1 \mu\text{m: } \alpha = 1.5 (L/L_0) - 0.5$$

$$\text{For } L \geq 1 \mu\text{m and } L \leq 1.1 \mu\text{m: } \alpha = 1.0 \quad (14)$$

$$\text{For } L > 1.1 \mu\text{m: } \alpha = -1.6 (L/L_0) + 2.76$$

The titin function ($KTitin$; Eq. 15) expresses the SL-dependent change of the spacing between the actin and myosin filaments caused by titin-based radial force in the physiological SL range of the heart (Eq. 16) and the damage of titin at SLs greater than $2.2 \mu\text{m}$ (Eq. 17) [14]. The latter part (Eq. 17) is not relevant concerning the physiological working range of the heart. In contrast to nature, in the model titin damage is reversible.

$$KTitin = \begin{cases} f_{titinNormal} & (L \leq 1.1 \mu\text{m}) \\ f_{titinDamaged} & (L > 1.1 \mu\text{m}) \end{cases} \quad (15)$$

$$f_{titinNormal} = kTitin \frac{6.8753}{1 + e^{((-L/L_0)+0.9601)/0.0449}} \quad (16)$$

$$f_{titinDamaged} = kTitin (-31.0 (L/L_0) + 40.0) \quad (17)$$

The force generating step (Q_{Fgen}) is characterized by a fast conformational change of the actin bound myosin, which opens the P_i binding pocket and results in a strong Xb state. The net rate is given by:

$$Q_{Fgen} = k_3 [RUAMADPPi] - k_{-3} [RUAM_ADPPi] \quad (18)$$

The rate parameter for this conformational change (k_3) changes due to positive cooperativity caused by activated RUs (first term in Eq. 19) and negative cooperativity caused by strong Xbs (second term) as follows: (19)

$$k_3 = k_{3c} \left[1 + k_{3f} \left(\frac{[RUTCaon]_{eff} + [RUTMon]_{eff} + [RUAMADPPi]}{[RU_{total}]} \right) \right]^2 \times$$

$$\left[1 + k_{3sb} \frac{([RUA_MADPPi] + [RUA_MADP])^2}{[RU_{total}]} \right] \times [RUTCaon]_{eff} = \alpha [RUTCaon] \quad (20)$$

The net rate of the P_i release (Q_{PiR}) is expressed as:

$$Q_{PIR} = k_4 [RUA_MADPPi] - k_{-4} [RUA_MADP] \quad (21)$$

The net rate of the ADP release (Q_{ADPR}) is given by:

$$Q_{ADPR} = k_5 [RUA_MADP] \quad (22)$$

In isometric contractions (load fraction 1) the ADP release is the rate limiting step of the Xb cycle with a constant k_5 value depending on the PL (Table 1). In isotonic contractions the k_5 value is PL and AL-dependent (see section "Simulations of Afterloaded Isotonic Contractions").

The rate changes for the different RU species and $[Ca^{2+}]$ are determined as follows:

$$d[RUTCaoff]/dt = Q_{CaB} - Q_{TCaA} \quad (23)$$

$$d[RUTCaon]/dt = Q_{TCaA} - Q_{TMA} \quad (24)$$

$$d[RUTMon]/dt = Q_{TMA} - Q_{MB} + Q_{ADPR} \quad (25)$$

$$d[RUAMADPPi]/dt = Q_{MB} - Q_{Fgen} \quad (26)$$

$$d[RUA_MADPPi]/dt = Q_{Fgen} - Q_{PIR} \quad (27)$$

$$d[RUA_MADP]/dt = Q_{PIR} - Q_{ADPR} \quad (28)$$

$$d[Ca^{2+}]/dt = -Q_{CaB} \quad (29)$$

The active force (F_b) is proportional to the number of developed Xbs with A_f being the force factor [11].

$$F_b = A_f ([RUA_MADPPi] + [RUA_MADP]) \times (L - X) \quad (30)$$

The $(L-X)$ term implies a change of the average Xb force with load (see Eq. 32 below). The external force ($F_{ext} = \text{load}$) is defined as

$$F_{ext} = F_b + F_p \quad (31)$$

Cross-bridge Mechanics and Active Force

For the Xb mechanics the equation developed by Negroni and Lascano [11] was used, which describes the velocity for the movement of the mobile Xb end (dX/dt):

$$dX/dt = B \times (h - h_c) \quad \text{with} \quad h = L - X \quad (32)$$

where h is defined as the Xb elongation, h_c the steady state Xb elongation, X the part of L , which is not covered by h , and B as a proportionality factor. Analysis of force step simulations revealed a change of the h_c value with temperature and a B value change with load as shown in the next section.

Force Step Simulations to Adjust the h_c and B Parameter Values

A force step, which is initiated through a fast reduction of load from a muscle in the tetanic steady state, results in SL shortening characterized by four different phases [5]. Xb mechanics is clearly distinct from the kinetics in the elastic phase (P1) and the fast shortening phase (P2). X-ray diffraction data from frog skeletal muscle demonstrated that during P1 and P2 myosin heads move towards the center of the sarcomere, but no detachment and reattachment of Xbs was found [22]. To represent this behavior, in the force step

simulations during P1 and P2 the myosin binding rate parameter (k_{12}) and the ADP release rate (k_5) were set to zero. Simulations of P1 and P2 allowed allocating a physiological value and a biological meaning to the parameters h_c and B of the mechanics equation (Eq. 32). Since the only available experimental force step data from frog skeletal muscle recorded at 5°C [5] were not appropriate for model adjustment, the slow shortening phase (P3) and the steady state shortening phase (P4) were not analyzed.

Simulations were essentially performed as reported for force steps of frog skeletal muscle fibers [5]. First the tetanic steady state values for all variables and parameters were determined using the isometric model with a constant $[Ca^{2+}] = 2 \mu\text{M}$ and $L = 1.05 \mu\text{m}$. A force step simulation experiment was started from the tetanic steady state through a change from the isometric contraction model, i.e., $F_{ext} = 0$ and $F_b = -F_p$, to the isotonic model. Within one time step (0.001 ms) F_{ext} was set to account for the desired load as follows:

$$F_{ext} = \text{loadfraction} \cdot T_0 \quad (33)$$

with T_0 being the tetanic tension. In contrast, in the experiments the force step took 0.150 ms to be complete [5]. Simulation results for the P1 and P2 L shortening time courses for 5°C and 37°C are shown in Fig. (2A) and (2B), respectively.

Temperature Dependence of the Phase 1 Elastic Stroke

X-ray diffraction data from frog skeletal muscle fibers revealed that a rise in temperature from 0°C to 17°C causes the light-chain domain of the myosin heads to tilt axially, and the interference distance to decrease [23]. This observation led to our hypothesis that the length of the tilting myosin heads might be represented in the mechanics equation (Eq. 32) as h_c , and therefore, h_c should increase with an increase in temperature. In force step simulations a variation of h_c resulted solely in a change of L_1 , the length change due to the elasticity of the muscle. From the simulation data L_1 was taken as the length of L immediately after the force step as indicated in Fig. (2A). Experimental data revealed a temperature dependence for L_1 (Fig. 2C, symbols) [24]. The h_c value, which was determined by simulations to match the experimental L_1 value for a specific load and temperature, could reproduce L_1 values for other load fractions at the same temperature (Fig. 2C, lines). For a good match to experimental data, h_c was determined as 3.6 nm for 5°C and 5.0 nm for 17°C. Due to the lack of experimental data from cardiac muscle, h_c was adjusted to match data obtained from skeletal muscle, although cardiac muscle was found to be stiffer than skeletal muscle fibers [19,25].

A change of h_c in the isometric contraction model [14] inserted into the Kyoto Model [16] (see section "Simulations and Data Analysis") produced a change of F_b (Fig. 2D). However, the rise of F_b with an increase of h_c was not accompanied by a change of the $[Xb]$ (insert in Fig. 2D). Under isometric conditions, h_c is equal to $(L-X)$ (Eq. 30), and consequently, a higher h_c results in a larger F_b . This coincides with experimental findings that show a rise in active tension with increasing temperature without a change in stiffness [23,26]. It was concluded that the higher force is due to the higher strain in the head producing a higher force per Xb [23].

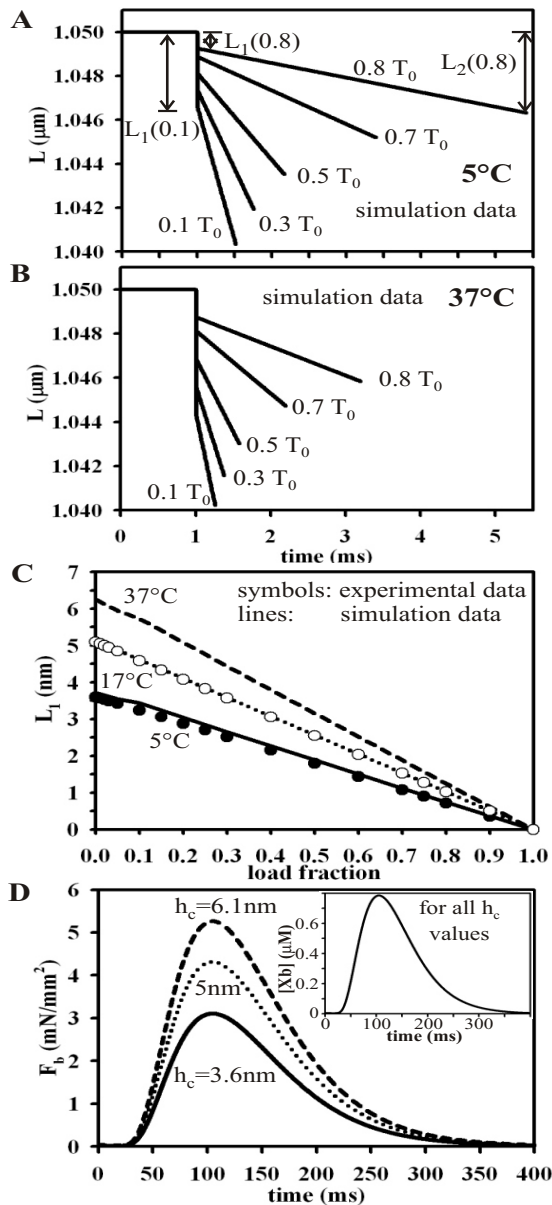


Fig. (2). Temperature dependence of the force step elastic shortening phase (P1). The L shortening time course from simulations of force steps (P1 and P2) is shown in panel **A** for 5°C and in **B** for 37°C. The numbers indicate load fractions. In panel **A** L_1 for load fraction 0.1 and 0.8 and L_2 for load fraction 0.8 are indicated by arrows. In panel **C** experimental data from frog skeletal muscle fibers (symbols) [24] for the load and temperature dependence of L_1 are compared to simulation results (lines). Panel **D** shows the alteration of the F_b time course from isometric twich contractions ($L=1.05 \mu\text{m}$) with a change of h_c . Data were obtained from the isometric model inserted into the Kyoto Model [16]. The insert in **D** shows the identical $[Xb]$ time course for all h_c values.

A linear increase of h_c with temperature causes a linear rise of F_b with temperature. However, experiments showed that F_b rises linearly with temperature up to about 17-20°C,

but reaches a plateau at higher temperatures [27]. Therefore, h_c for 37°C, the desired temperature for the contraction model, was set to 6.1 nm to match the experimentally found non-linear F_b -temperature relation. In conclusion, simulation results allow attributing h_c to the length of the myosin head and its temperature-dependent elastic changes.

The Factor B Determines Phase 2

P2 is characterized by a fast linear shortening of L (Fig. **2A** and **2B**) to L_2 , the sum of the elastic and the working stroke (L_T), which are related as follows:

$$L_T = L_2 - L_1 \quad (34)$$

From the only available force step experimental data set consisting of the shortening velocity of P2 (V_2) (Fig. **3A**), solid line with filled circles) and L_T (Fig. **3B**, filled triangles) from frog skeletal muscle (5°C) [5], the duration of P2 (t_2) for each load was calculated as follows (Fig. **3A**, dotted line with filled circles):

$$t_2 = L_T / V_2 \quad (35)$$

Using t_2 the model could be adjusted to match the V_2 data through a change of B with load (Eq. 32), resulting in L_2 and L_T for 5°C as depicted in Fig. **3B** (L_2 : solid line; L_T : dashed line). L_2 was determined from the simulation data as the amount of shortening attained at the end of P2 (Fig. **2A**). In contrast, in the experiments L_2 was measured graphically using a tangent on the P3 shortening time course [5]. This method, however, results in a L_2 value which is highly dependent on the P3 shortening time course. The slight divergence from experimental data is probably due to the different method used to determine L_2 . V_2 was determined from simulation data through a linear regression analysis of a time versus L plot over the whole period of P2, which is linear (Fig. **2A** and **2B**). The obtained B -load relationship for 5°C is shown in Fig. **3C** (filled circles).

Due to the lack of 37°C experimental force step data from cardiac muscle which include P2, some assumptions were necessary to develop a B -load relationship. L_T was set to 4 nm independent of load, since experiments revealed that L_T gets load independent at higher temperature [24]. Although having the unit [1/ms], B is not equal to $1/t_2$. As the factor for dX/dt , B is defined as

$$B = \frac{dX}{dt} \times \frac{1}{(L - X - h_c)} \quad (36)$$

This equation could be discretized as follows to apply simulation data:

$$B = \frac{X_{P2end} - X_{P2start}}{t_2} \times \frac{1}{L_{P2mid} - X_{P2mid} - h_c} = \frac{c}{t_2} \quad (37)$$

with $X_{P2start}$, X_{P2mid} and X_{P2end} being X at the start, middle and end of P2, respectively and L_{P2mid} , L at the middle of P2. The value of c depends on h_c (Eq. 37) and L_T . But according to $c = B \times t_2$, c is valid for various B - t_2 combinations. This allows the calculation of c from preliminary simulation data, which were obtained with $h_c = 6.1 \text{ nm}$, B values from 5°C, and L_T adjusted to 4 nm through a change of t_2 . To calculate

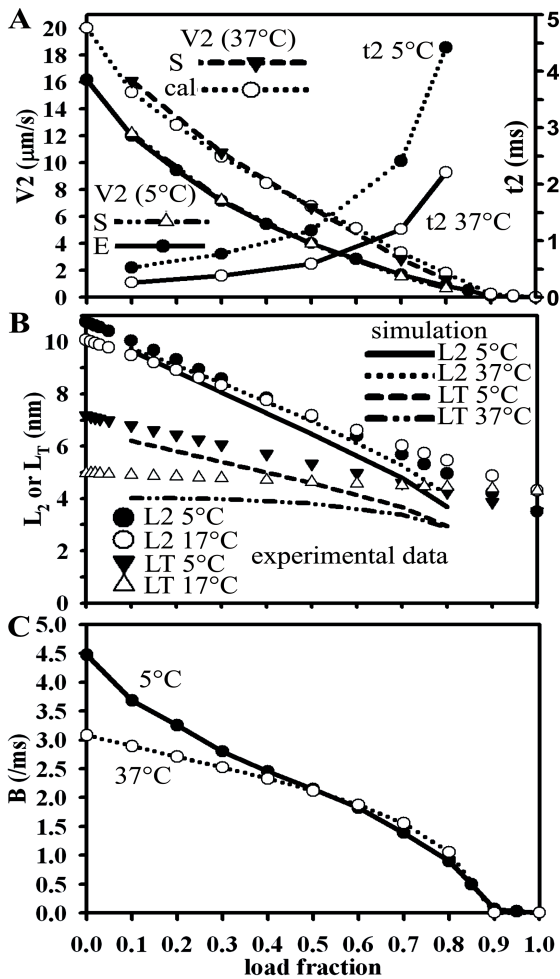


Fig. (3). Characterization of the force step fast shortening phase (P2). Panel A shows V2 data from 5°C frog skeletal muscle experiments [5] (solid line with filled circles, labeled E) compared to V2 data obtained from 5°C simulations (open triangles, labeled S) using the calculated t_2 (5°C) data (dotted line with filled circles). For 37°C simulations the assumed t_2 data (solid line with open circles) were used. Simulation results for V2 (37°C) (filled triangles, labeled S) are compared to calculated V2 data (dotted line with open circles, labeled cal). Experimental data from frog skeletal muscle for 5°C and 17°C (symbols) [24] and the simulation results for 5°C and 37°C (lines) for the load dependence of L_2 and L_T are shown in B. The obtained B-load relationships are depicted in C.

the B values from these calculated c values, t_2 was assumed to be 50% of t_2 from frog (5°C) (Fig. 3A, solid line with open circles). The dominant cardiac muscle myosin heavy chain (MHC) in healthy rodent hearts, α , is significantly slower than the fast skeletal muscle MHC isoforms [28]. However, the temperature difference of 32°C was taken into account. From the calculated c and the assumed t_2 values, B for 37°C was calculated ($B=c/t_2$). Then V2 was determined as follows (Fig. 3A, dotted line with open circles):

$$V2 = B \cdot L_T / c \quad (38)$$

which gave similar results to V2 determined from simulation data using B and t_2 (Fig. 3A, dashed line with filled trian-

gles). The B-load relation for 37°C as shown in Fig. 3C (open circles) was fitted as follows:

$$\text{load} \leq 0.9: \quad B = \frac{3.08 - 3.42 \text{ load}}{1 - 0.48 \text{ load} - 0.44 \text{ load}^2} \quad (39)$$

$$\text{load} > 0.9: \quad B = 0.006$$

A decreasing B with increasing load implies a decrease of V2 with load. A change of B with load under steady state shortening was found to increase model stability. Due to h_c , c is temperature-dependent (Eq. 37), and therefore B. Since no Xb attachment and detachment occurs in P2, V2 is only determined by the myosin isoform. Hence, B represents the myosin isoform characteristic. A change of B might be necessary with an isoform shift which is sometimes found in the diseased heart [29]. L_2 represents the maximum possible extension of the myosin head before detachment and is about 11 nm at low load independent of temperature (Fig. 3B) [24]. In conclusion, the Xb mechanics is satisfactorily described by Eq. 32.

Simulations of Afterloaded Isotonic Contractions

Simulations of afterloaded isotonic contractions were performed based on cat papillary muscle experiments [2]. In these experiments the muscle was first stretched by a small weight, the PL, to a length consistent to its resting LTR. This length was then fixed, so that the muscle did not sense any additional added weight, the AL, until it started to contract. For the simulations the resting L was determined by setting the PL equal to F_{ext} . A 40 nM resting $[Ca^{2+}]$ was used. The isometric model combined with a simple SR model (see section "Simulations and Data Analysis") was used to determine the maximum F_b for the given PL. The maximum F_{ext} (F_{extmax}), which is the force at which the muscle cannot shorten any longer (isometric contraction), was defined as

$$F_{\text{extmax}} = F_p + F_{b\text{max}} \quad (40)$$

and used to calculate the load fractions

$$\text{load} = F_{\text{ext}} / F_{\text{extmax}} \quad \text{with} \quad F_{\text{ext}} = PL + AL \quad (41)$$

Shortening velocity was calculated for each time step from the change of L during the time step:

$$V = \Delta L / \text{time step} \quad (42)$$

The peak shortening velocity was used for the FVR. At times where L was constant, i.e., no shortening, all load-dependent parameters were set to the isometric value, i.e., load fraction = 1. The B-load relation (Eq. 39) was used, and h_c set to 6.1 nm.

For model analysis three PLs were chosen: PL 0, i.e., 0 mN/mm² (resting L = 0.95 μ m; F_{extmax} = 5.91 mN/mm²); PL 0.51 (1.0 μ m; 8.38 mN/mm²); PL 2.25 (1.0504 μ m; 10.89 mN/mm²). The availability of appropriate experimental data for model adjustment is very limited. Although cat papillary muscle experimental data for different PLs and ALs are available [2], only velocities for the muscle length changes given in (mm/s) were measured and plotted against the force in gram (Fig. 4A). Furthermore, these data were obtained

before it became obvious that damage to the ends of papillary muscles during preparation could cause artifacts in measurements [30]. Taking the shape of the experimental FVR (Fig. 4A) as reference, data to fit the PL 2.25 model were designed (Fig. 4B, filled squares). To adjust the unloaded shortening velocity (V_{max}) of the model, experimental data obtained from cat trabeculae ($V_{max} = 8.2 \mu\text{m/s}$, 25°C) [4] and guinea pig single myocytes ($V_{max} = 6 - 12.4 \mu\text{m/s}$, 35°C) [18] were taken as reference values. The shape of the FVR is influenced by many factors such as SL, $[\text{Ca}^{2+}]$, temperature, the MHC isoform [29], artifacts in measurements [30] and especially, depends on the type of the experiment performed and the time velocity is measured [2,4]. Generally, the FVR obtained from afterloaded isotonic contractions is less hy-

perbolic than the FVR obtained from force step experiments (insert in Fig. 4A). Due to the great variation with changing conditions, assuming physiological data for model fitting should be justified. Fitting was achieved through a variation of the ADP release rate (k_5) with different ALs. k_5 was chosen since it is the rate limiting step in the Xb cycle, and experimental data suggest the ADP release to be load-dependent (see discussion). At load fraction 1 (AL = 8.64 mN/mm^2) $k_5 = 0.0372306 / \text{ms}$ was used to give F which matches F_{extmax} . At load 1 the ADP release rate should have its minimum value, since more Xbs are necessary to bear the load. Naturally, an increasing k_5 rate parameter would be expected with a decrease in load. However, k_5 rapidly decreased for load fractions smaller than 0.35 (Fig. 5A, filled squares, labeled $k_5\downarrow$). A steadily increasing k_5 -load curve was designed for low load as shown in Fig. (5A) (dotted line with open circles) and fitted as follows:

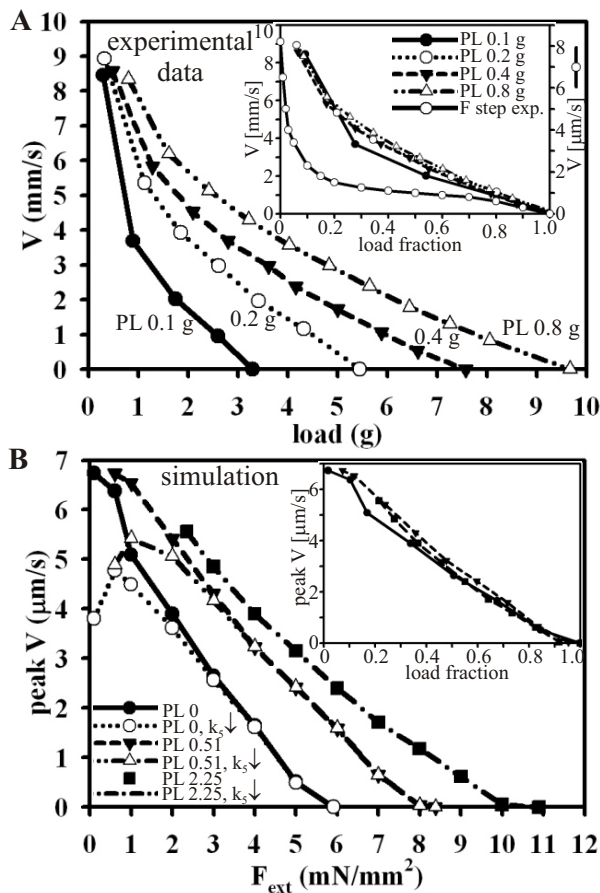


Fig. (4). Force-velocity relationship. Panel A shows experimental data for the FVR obtained for various PLs and ALs from cat papillary muscle [2]. The temperature was not given, but this group performed most experiments at 25 or 30°C . The FVR is PL dependent but plotting against the load fraction results in a single FVR (insert in A). A more hyperbolic FVR was obtained from force step experiments performed with cat trabeculae at 25°C (insert in A; solid line with open circles) [4]. FVR simulation results for PL 0, 0.51 and 2.25 for the original model (M1) and the model variant which uses $k_5\downarrow$ are shown in B. For PL 2.25, data from M1 and $k_5\downarrow$ are identical. The insert in B shows the M1 data plotted against the load fraction.

$$\text{For load} < 1: k_5 = 0.1419 - (0.2449 \text{ load}) + (0.1892 \text{ load}^2) - (0.0489 \text{ load}^3) \quad (43)$$

$$\text{For load} = 1: k_5 = 0.0373206$$

Using this relationship the model was then adjusted for low load to the desired shortening velocity by changing the speed of the Tm conformational change rate (k_{tmon}), the rate limiting step in the thin filament activation, using the factor k_{loadTM} . The k_{loadTM} -load relationship shown in Fig. (5B) (filled triangles) was fitted as follows:

$$\text{PL 2.25: For load} < 0.36725: k_{loadTM} = 0.9652 + 3.2044 e^{(-12.3147 \text{ load})} \quad (44)$$

$$\text{For load} \geq 0.36725: k_{loadTM} = 1.0$$

The attained end-systolic L (L_{min}) decreased linear with a decrease in AL as depicted in Fig. (6A) (filled triangles). Experimental data from cat papillary muscle revealed that for different PLs, but for the same final loads ($F_{ext} = PL + AL$), the muscle shortened to the same end-systolic muscle length [31]. In addition, isolated intact cardiac myocytes from guinea pig shortened to the same end-systolic cell length or SL at 37°C despite different PLs if loaded with the same total load [32]. Based on these findings, using the F_{ext} - L_{min} relationship obtained from PL 2.25 (Fig. 6A), the models for PL 0 and PL 0.51 were fitted to match this relationship. For PL 0.51 $k_5 = 0.0546543 / \text{ms}$ and for PL 0 $k_5 = 0.05439 / \text{ms}$ were determined for load fraction 1. Again k_5 was found to decrease at low load (Fig. 5A, filled (PL 0) and open (PL 0.51) triangles; labeled $k_5\downarrow$). A constantly rising k_5 with a decrease of load was designed which was appropriate for PL 0 and 0.51 (Fig. 5A, filled circles).

$$\text{For load} \leq 0.8275: k_5 = 0.0317 + 0.2035 e^{(-2.5623 \text{ load})} \quad (45)$$

$$\text{For } 0.8275 < \text{load} < 1: k_5 = 0.0668 - (0.0168 \text{ load}) + (0.0047 \text{ load}^2)$$

For low load both PL models were adjusted to the L_{min} as determined for PL 2.25 with a change of k_{tmon} using the factor k_{loadTM} (Eq. 10). The k_{loadTM} -load relationships for PL 0

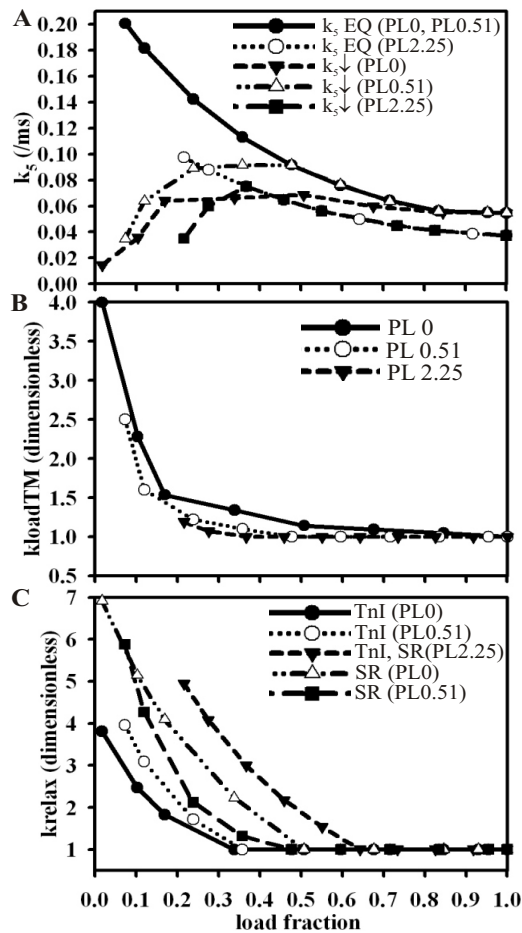


Fig. (5). Load dependence of rate parameters. The load dependence of the ADP release rate, k_5 , is shown in **A**. EQ indicates that the results are from the fitted equation, Eq. 43 (PL 2.25) and Eq. 45 (PL 0 and 0.51). Results from the fitted equations Eq. 44, Eq. 46 and Eq. 47 for the load-dependent change of the Tm conformational change rate by the factor k_{loadTM} are shown in **B**. The load-dependent changes of the TnI conformational change to the “off” conformation (k_{off}) (labeled TnI; Eq. 50-52) and the increase in the SR Ca^{2+} uptake (labeled SR; Eq. 57-59) during relaxation are depicted in panel **C**.

(filled circles; Eq. 46) and PL 0.51 (open circles; Eq. 47) are shown in Fig. (5B).

$$\text{PL 0: For load} \leq 0.169: k_{loadTM} = 0.3464 + 4.1391 e^{(-7.3778 \text{ load})} \quad (46)$$

$$\text{For } 0.169 < \text{load} < 0.5111: k_{loadTM} = 1.732 - 1.1619 \text{ load}$$

$$\text{For load} \geq 0.5111: k_{loadTM} = 1.2811 - 0.2797 \text{ load}$$

$$\text{PL 0.51: For load} \leq 0.2396: k_{loadTM} = 1.2 + 8.2241 e^{(-25.3513 \text{ load})} \quad (47)$$

$$\text{For } 0.2396 < \text{load} < 0.47727: k_{loadTM} = 1.52 - (1.4248 \text{ load}) + (0.7024 \text{ load}^2)$$

$$\text{For load} \geq 0.47727: k_{loadTM} = 1.0$$

For all PLs during relaxation ($V < -0.5 \mu\text{m/s}$): $k_{loadTM} = 1.0$.

To obtain a high velocity for very low load a steeper shortening than expected from the linear L_{min} - F_{ext} relation was necessary (Fig. 6A). According to the FLR form cardiac muscle the minimum SL is around $1.7 \mu\text{m}$ [33], although smaller SLs were measured in isolated cardiac myocytes [18]. To compromise velocity, shortening in the model was limited to $1.6 \mu\text{m}$. With a change of any other rate parameter (k_{off} , k_{12} , k_3) instead of k_{tmon} , an adjustment to a high velocity at low load was not possible, even with much deeper shortening.

Relaxation Mechanisms

To speed up isotonic relaxation three mechanisms were considered: SL-dependent titin restoring force, TnI in the “off” conformation pulling Tm to the “off” state and a load-dependent change of k_{off} effective at low load. Titin was shown to play a role during early diastole in the heart [21]. Shortening of the sarcomere below slack length causes the elastic titin spring to be coiled up at the Z disc [20]. This stored elastic energy is released as restoring force during relaxation and was measured as sarcomere relengthening velocity [21]. The molecular mechanism, how the restoring force acts to turn off muscle contraction, is unknown [21,34]. Here, it was assumed that this force disrupts the structure of the head-to-tail combined Tm molecules (see discussion). During relaxation this is expressed as a faster change of Tm molecules to the “off” conformation for SL below slack length. Independent of the PL for $L < 0.95 \mu\text{m}$ during relaxation ($V < -0.5 \mu\text{m/s}$; this value was chosen instead of $V < 0$ for a good model stability.), k_{tmon} , the conformational change rate for Tm to the “off” state, (Eq. 10) was multiplied by:

$$\text{titinRF} = -16.0 (L/L_0) + 16.2 \quad (48)$$

with L_0 a normalization factor. The steepness of this equation, i.e., the effect of titin’s restoring force, is arbitrary. A linear relationship was chosen, because the SL- relengthening velocity relationship was reported to be linear [21]. Nevertheless, titin’s influence is small, since it effects relaxation only if the sarcomere is below slack length.

According to a published model which is based on structural evidence [35], TnI molecules in the “off” conformation pull Tm molecules to the “off” conformation. To account for this cooperativity effect in the present model, during relaxation k_{tmon} (Eq. 10) was increased through the factor k_{offTnI} with an increase of the TnI concentration in the “off” conformation, $[RUTCaoff]$, as follows:

$$k_{offTnI} = (1 + k_{offrelax} [RUTCaoff]/[RUtotal])^2 \quad (49)$$

This change was independent of the applied PL.

At low load for a good late relaxation, a change of the TnC Ca^{2+} affinity through an increase in the rate of the TnI conformational change to the “off” conformation (k_{off}) was essential. During relaxation k_{off} was multiplied by the factor

$k_{relaxTn}$ (Eq. 7), which is load and PL-dependent as depicted in Fig. (5C) (PL0 (filled circles), PL 0.51 (open circles), PL 2.25 (filled triangles)). The fitted equations used for $V < -0.5$ $\mu\text{m/s}$ are as follows:

$$\text{PL 0: For load fraction} < 0.338229: k_{relaxTnI} = 0.5447 + 3.617 e^{(-6.1125 \text{ load})} \quad (50)$$

$$\text{For load fraction} \geq 0.338229: k_{relaxTnI} = 1.0$$

$$\text{PL 0.51: For load fraction} < 0.35795: k_{relaxTnI} = 0.3774 + 5.5067 e^{(-5.9271 \text{ load})} \quad (51)$$

$$\text{For load fraction} \geq 0.35795: k_{relaxTnI} = 1.0$$

$$\text{PL 2.25: For load fraction} < 0.6427: k_{relaxTnI} = -0.5639 + 10.2568 e^{(-2.8761 \text{ load})} \quad (52)$$

$$\text{For load fraction} \geq 0.6427: k_{relaxTnI} = 1.0$$

$$\text{For all PLs during shortening} (V \geq -0.5 \mu\text{m/s}): k_{relaxTnI} = 1.0.$$

Simulations and Data Analysis

The contraction model was implemented in Java using the simBio package [36], software for cell simulation. The differential equations were solved using an Euler method with dynamically adjusted time steps. The bisection method from “Numerical Recipes” [37] was used to determine L in each time step. The original model is referred to as M1, and the model which lacks the titin function as M2 [14]. In M2 Eq. 12 was exchanged to Eq. 53.

$$Q_{MB} = k_{12} [MADPPi] \times [RUTMon]_{eff} - k_{-12} [RUAMADPPi] \quad (53)$$

For steady state simulations a constant $[Ca^{2+}]$ was used. Two different ways to obtain a Ca^{2+} transient were employed. For the twitch contractions (Fig. 2D) and the isotonic contractions (see Fig. 11) the Kyoto Model, a guinea pig based cardiac myocyte model [16], Ca^{2+} transient was used. For simulations of afterloaded contractions a simple sarcoplasmic reticulum (SR) model [11] was applied. Q_{rel} describes the Ca^{2+} release from the SR and Q_{pump} the Ca^{2+} uptake into the SR.

$$Q_{rel} = Q_m \times (t/t_p)^4 \times e^{4(1-t/t_p)} + Q_{pumprest} \quad (55)$$

$$Q_{pump} = k_{relaxSR} \times K_p / \left(1 + (K_m / [Ca^{2+}])^2 \right) \quad (56)$$

with K_m a SR pump parameter, K_p the maximum value of Q_{pump} , $Q_{pumprest}$ the value of Q_{pump} under resting $[Ca^{2+}]$ conditions, Q_m the maximum value of Q_{rel} and t_p the time to Q_m . For simulations which include the SR model, the Ca^{2+} uptake into the SR was enhanced during relaxation at low load expressed in Eq. 56 by the load-dependent factor $k_{relaxSR}$. This load dependent enhancement was necessary due to the lack of Ca^{2+} buffers others than TnC in the simple system. In myocytes many Ca^{2+} buffers operate to avoid sudden $[Ca^{2+}]$ changes. Thus, there is no physiological relevance for this load-dependent mechanism. No change was applied to the Ca^{2+} SR uptake in the Kyoto Model which includes a Ca^{2+} buffering system [16]. The $k_{relaxSR}$ -load relationships shown

in Fig. (5C) (PL 0: open triangles; PL 0.51: filled squares; PL 2.25: filled triangles) are as follows:

$$\text{PL 0: For load fraction} < 0.50734: k_{relaxSR} = -0.3585 + 7.6714 e^{(-3.2215 \text{ load})} \quad (57)$$

$$\text{For load fraction} \geq 0.50734: k_{relaxSR} = 1.0$$

$$\text{PL 0.51: For load fraction} < 0.59659: k_{relaxSR} = -0.4531 + 7.8531 e^{(-2.7168 \text{ load})} \quad (58)$$

$$\text{For load fraction} \geq 0.59659: k_{relaxSR} = 1.0$$

$$\text{PL 2.25: For load fraction} < 0.6427: k_{relaxSR} = -0.5639 + 10.2568 e^{(-2.8761 \text{ load})} \quad (59)$$

$$\text{For load fraction} \geq 0.6427: k_{relaxSR} = 1.0$$

$$\text{For all PLs during shortening} (V \geq -0.5 \mu\text{m/s}): k_{relaxSR} = 1.0.$$

For the calculation of the $[Ca^{2+}]$ change with time, Eq. 60 was used instead of Eq. 29.

$$d[Ca^{2+}]/dt = Q_{rel} - Q_{pump} - Q_{CaB} \quad (60)$$

Mathematical equations used for fitting of the obtained relationships for the load dependence of rate parameters were chosen to give the best possible fit. Mainly equations of the type rational, polynomial or exponential decay were employed. In the case a good fit with the software SigmaPlot (version 10.0; Systat Software, Inc.) with just one equation was not possible, two equations were fixed together at the cutting point, which was determined using MatLab (version 7.3.0.267 (R2006b); The MathWorks, Inc.). The model was quite sensitive concerning the value of load-dependent factors. Therefore, four or more decimal places were required in same cases.

RESULTS

Regulation of Shortening and Velocity

The effect of load on the Xb kinetics during shortening at 37°C was studied with simulations of afterloaded isotonic contractions for PL 0, PL 0.51 and PL 2.25 (in mN/mm^2). Adjustment of the PL 0 and PL 0.51 models (see Method) to reach the same end-systolic L (L_{min}) for the same total load as determined for PL 2.25 (Fig. 6A, M1), resulted in the FVR (Fig. 4B) as expected from experiments (Fig. 4A). Moreover, regardless of the PL the same peak $[Xb]$ was attained for the same total load (Fig. 6B, M1). Results for the force, L, $[Xb]$ and velocity time courses for PL 2.25 with various ALs are shown in Fig. (7A), (7B), (7C) and (7D), respectively. For a given PL, the smaller the AL the greater is the amount of shortening, but the faster is the time to L_{min} and the higher is the maximum velocity.

A comparison between PL 0, 0.51 and 2.25 for $F = 4$ mN/mm^2 is presented in Fig. (8). The different PL models were adjusted to the same L_{min} for the same force as confirmed in Fig. (8A) and Fig. (8B). The higher the PL the faster was the shortening velocity to reach L_{min} (Fig. 8C). The total $[Xb]$ reaches about the same maximum regardless

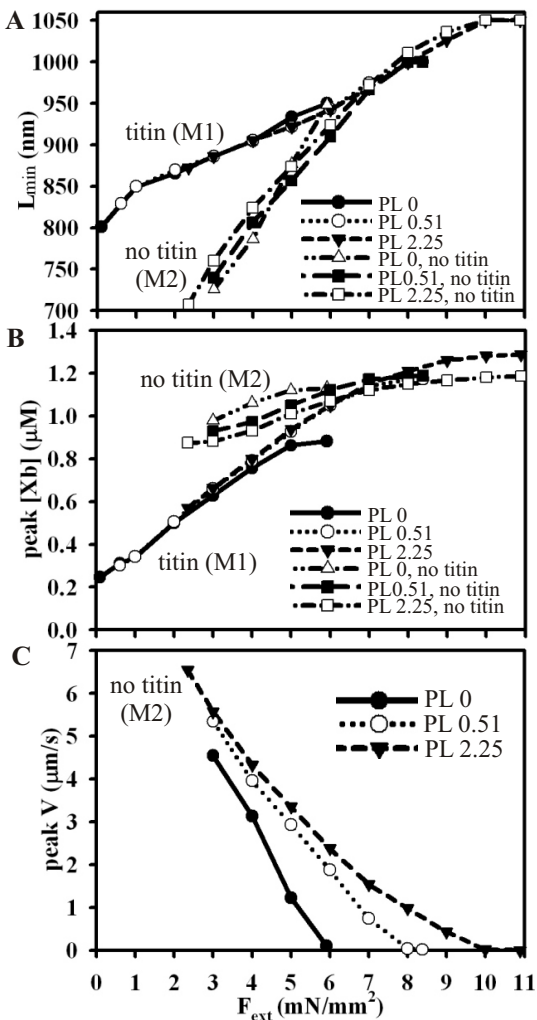


Fig. (6). Simulation results from afterloaded isotonic contractions for M1 and M2. In panel **A** L_{\min} and in panel **B** the peak $[Xb]$ are plotted against F_{ext} for M1, the original model with titin-based radial force, and M2, the model which lacks titin, labeled as “no titin”. Panel **C** shows the FVR simulation results for M2.

of the PL (Fig. 8D). Since for the same L_{\min} F_p is the same, F_b has to be the same to satisfy Eq. 31. The small difference of the peak $[Xb]$ is due to the $(L-X)$ term in Eq. 30. The minimum of $(L-X)$ coincides with the peak of the $[Xb]$ (Fig. 8E) and the peak velocity (Fig. 8F). The higher the value of the $(L-X)$ minimum, the less Xb s are necessary to get to the same F_b , i.e., the more force has the average Xb (Fig. 8D and 8G). With an increase in the shortening velocity, the Xb force decreases (Fig. 8H), i.e., with an increase in load the average Xb force increases (insert in Fig. 8H). For PL 0 L_{\min} was reached with a delay (Fig. 8B). Due to the short SL the Xb -induced cooperative activation was reduced (smaller K_{Titin} , Eq. 16), which resulted in a slower activation of RUs (RUTMon) and a smaller fraction of effective RUTMon. Although the load-dependent change of the Xb force is small compared to the change of the $[Xb]$, it is essential, since a model with a constant $(L-X)$, i.e., F_b only dependent on $[Xb]$ was unstable and could not be adjusted to give the desired FVR (data not shown).

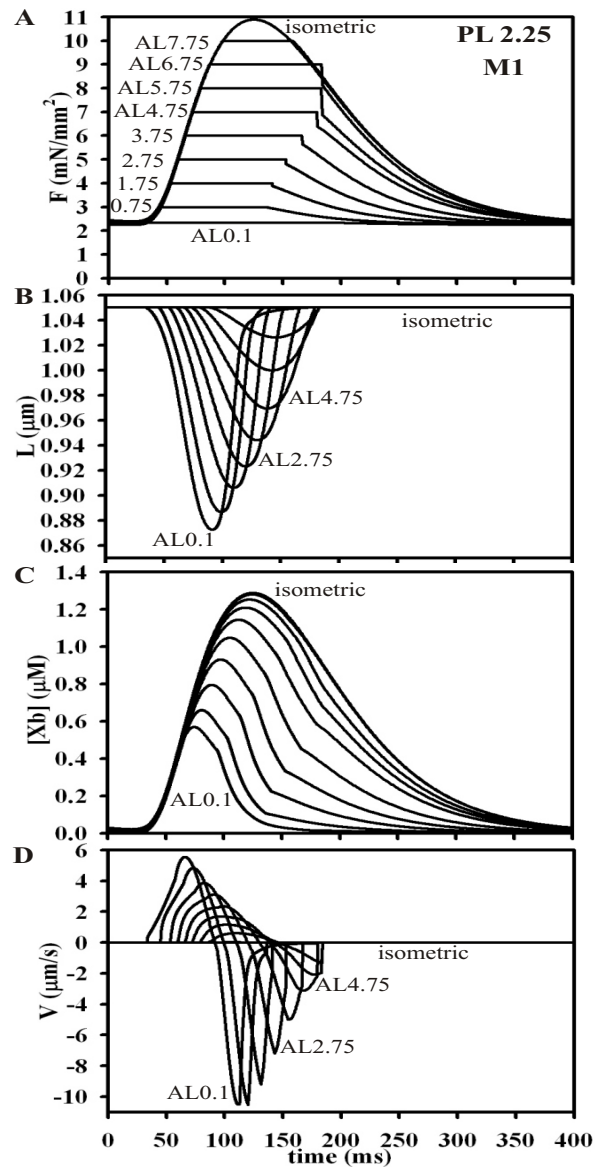


Fig. (7). Simulation results from afterloaded isotonic contraction with PL 2.25. For various ALs the time courses for force (**A**), L (**B**), $[Xb]$ (**C**) and the shortening and relaxation velocity (**D**) are shown. The model which includes all relaxation mechanisms was used for the simulations.

In conclusion, the ADP release rate controls the peak $[Xb]$ at high to medium load, the physiological working range of the heart, which corresponds to a velocity of up to about 5-6 $\mu\text{m/s}$ in the model (Fig. 9A). The peak $[Xb]$ decreases linearly with velocity in this range (Fig. 9A) as expected from a linear rise of k_5 with velocity (Fig. 9B). But at higher velocity a common value of about 0.3 μM is reached independent of the PL, suggesting that a physiological minimum is attained. The minimum $[Xb]$ is maintained through a faster activation of RUs achieved through an increase in the T_m conformational change rate mediated by the factor k_{loadTM} for velocities greater than 5 $\mu\text{m/s}$ (Fig. 9B). The Xb force, expressed by $(L-X)$, decreases linearly with a

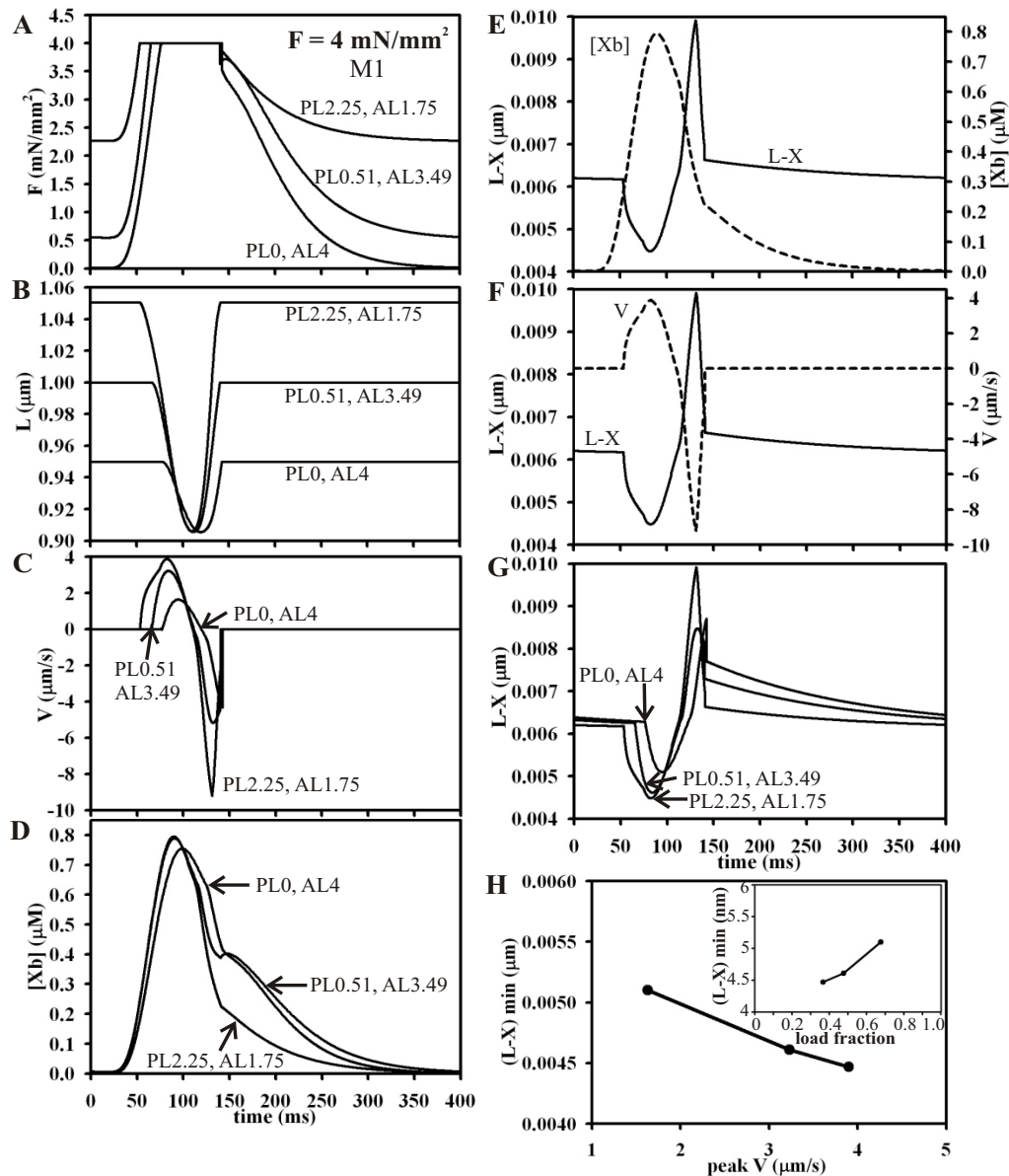


Fig. (8). Comparison of afterloaded isotonic contractions obtained with different PL models reaching the same total load $F=4 \text{ mN/mm}^2$. The time courses for force (A), L (B), velocity (C) and $[Xb]$ (D) are shown for the following load combinations: PL 0 with AL 4, PL 0.51 with AL 3.49 and PL 2.25 with AL 1.75. The minimum of $(L-X)$ coincides with the peak $[Xb]$ (E) and the maximum shortening velocity (F). Panel G shows the $(L-X)$ time courses for the three load combinations. The $(L-X)$ minima for the three load combinations are plotted against the peak velocity (H) or against the load fraction (insert in H).

rise in velocity (Fig. 9A), which is independent of the PL. However, this change is small compared to the change of $[Xb]$, suggesting that the FVR is mainly determined by the $[Xb]$ (Fig. 8C, 8G and 8H).

The Influence of Titin-Based Radial Force on Shortening and Velocity

To elucidate the effect of titin-based radial force on shortening and velocity, the SL-dependent influence of titin on the myosin binding rate was eliminated (M2), with no changes of the k_5 and k_{loadTM} -load relationships. Simulation results for PL 0, 0.51 and 2.25 are shown in Fig. (6). Although at high F_{ext} L_{min} obtained with M2 is similar to the

L_{min} reached with the titin model (M1), for smaller loads a much smaller L_{min} compared to M1 was found (Fig. 6A). The peak $[Xb]$ change with F_{ext} was very small for M2 (range: $0.875 \mu\text{M}$ to $1.186 \mu\text{M}$ for PL 2.25) compared to M1 (range: 0.57 to $1.288 \mu\text{M}$) (Fig. 6B). Due to the large shortening amount at smaller F_{ext} , the peak velocity is higher for M2 (Fig. 6C) compared to M1 (Fig. 4B). Our simulation results predict that titin-based radial force variations with SL prevent cardiac muscle to reach smaller SLs at medium to low load.

Fig. (10A) shows the PL 0.51 force time courses from afterloaded isotonic contractions for M1 and Fig. (10B) for M2. In the medium load range a decrease in AL was accom-

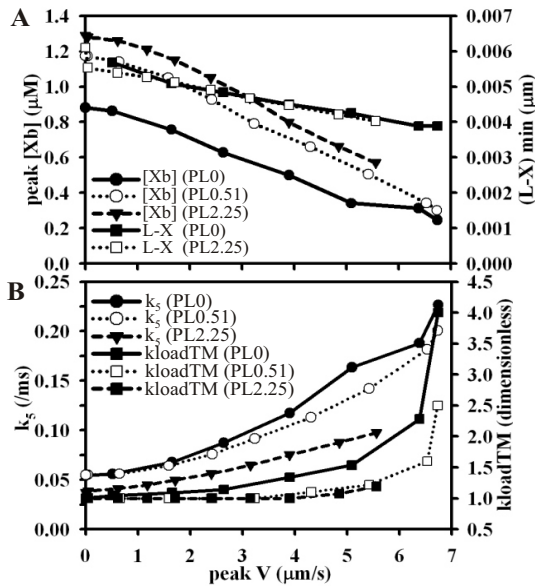


Fig. (9). The dependence of the peak [Xb] and the ADP release rate on the velocity. In panel **A** the peak [Xb] and (L-X) from afterloaded contractions obtained with the PL 0 and 2.25 models and in panel **B** k_5 and k_{loadTM} are plotted against the velocity.

panied by a faster start of the isometric relaxation in M1, but almost no change was found in results obtained with M2. The AL-dependent onset change of the isometric relaxation can be attributed to the shortening-induced cooperative deactivation in M1 which is missing in M2. Due to the SL-dependence of the myosin binding rate (k_{12}) caused by titin's radial force in M1, sarcomere shortening slows down k_{12} and therefore strong Xb formation, which in turn reduces thin filament activation via an increase in k_{off} (Fig. 1A) [14]. The smaller the AL the smaller is L_{min} and the faster is the deactivation. This deactivation reduces the shortening velocity in M1 as compared to M2 (inserts in Fig. 10A and 10B).

Analysis of Relaxation Mechanisms

Titin-based radial force in M1 prevents a fast isotonic relaxation speed (insert in Fig. 10A), since an increase in the SL promotes activation and delays force relaxation. This Xb-induced cooperative activation is missing in M2 (insert in Fig. 10B). To improve relaxation, which was reported to be faster than shortening [38], three mechanisms were considered (see Method): 1. a SL-dependent effect from titin restoring force, 2. TnI in the "off" conformation pulling Tm to the "off" state and 3. a load-dependent change of k_{off} only effective at low load.

Fig. (10C) exhibits force time course data for various ALs from simulations obtained with the PL 0.51 M1 that includes the above relaxation mechanisms. A slightly faster relaxation than shortening was achieved (insert in Fig. 10C). The time interval from stimulation to the onset of isometric relaxation (RST = relaxation start time) was chosen for model adjustment. A comparison of simulation data from relaxation-adjusted and unadjusted models with experimental data is shown in Fig. (10D). Except for the steepness of the slope, simulation data are comparable to experimental

data from cat. To achieve a faster velocity for relaxation than for shortening, the steeper relationship was necessary for the model. However, the steepness might depend on various factors such as temperature and stimulation frequency. As found in experiments, simulation results show a decrease in RST at very high load and an increase at very low load (Fig. 10D and 10E). For high ALs relaxation could be adjusted using only titin restoring force (Eq. 48) and the [RUTCaoff] cooperativity feedback mechanism (Eq. 49) as shown in Fig. (10F). As demonstrated in Fig. (10E), regardless of the PL, for the same F_{ext} the same RST was found. For lower loads, as indicated by arrows, a load-dependent increase of k_{off} (Eq. 50-52) was necessary. The higher the PL the stronger was this load dependence of the relaxation. The steepness of the slope is due to the strength of the titin restoring force and the pulling force TnI exerts on Tm. To show how each mechanism influences relaxation, simulations with modified models for PL 0.51 and AL 0.49 were performed. As depicted in Fig. (10G) (line with small dash) titin restoring force alone only speeds up the very early relaxation, whereas the [RUTCaoff] cooperativity feedback is more powerful in effecting the early relaxation (dash with two dots). However, at this low load for a fast late relaxation an increase of k_{off} was essential. A faster k_{off} rate indirectly enhances the Ca^{2+} release from TnC. If the Ca^{2+} transient was produced by a simple SR model without Ca^{2+} buffers, bumps in the Ca^{2+} transient occurred (Fig. 10H). In this case, an enhanced SR Ca^{2+} uptake was necessary at lower load to achieve full relaxation (Eq. 57-59). No bumps were observed if the myocyte model was employed due to Ca^{2+} buffering.

Model Validation- Isotonic Contractions in a Myocyte Model

With the Kyoto Model [16], which produces a more physiological Ca^{2+} transient, only simulations of non-afterloaded (AL=0) contractions are possible. Recently, it was reported that with an increase in PL the peak $[Ca^{2+}]_o$ increases in a range from $0.8 \pm 0.1 \mu M$ for PL 0 to $1.45 \pm 0.25 \mu M$ for optimal SL in rabbit trabeculae (37°C, 2Hz, 2.5 mM $[Ca^{2+}]_o$) [39]. In the present model adjustment of the peak $[Ca^{2+}]_o$ through a change of the L-type Calcium channel Ca^{2+} permeability [16] was found to be important to obtain a shortening amount which is comparable to experimental data. Fig. (11A) shows the simulation results for the isotonic shortening time courses for different PLs compared to experimental data. The shortening amount changes with PL as follows: PL 0, 8.2%; PL 0.51, 10.0%; PL 2.25, 11.9%. This is in the range found experimentally for guinea pig myocytes [18,40]. The Ca^{2+} transients are depicted in Fig. (11B). The normalized Ca^{2+} transients are very similar suggesting no influence in the relaxation (insert in Fig. 11B) as reported from experiments [39]. The velocity time courses are depicted in Fig. (11C) showing that relaxation velocities are faster than shortening velocities.

DISCUSSION

The present study stands out among other simulation studies performed to analyze the regulation of shortening and relaxation because of the unique cardiac muscle contraction

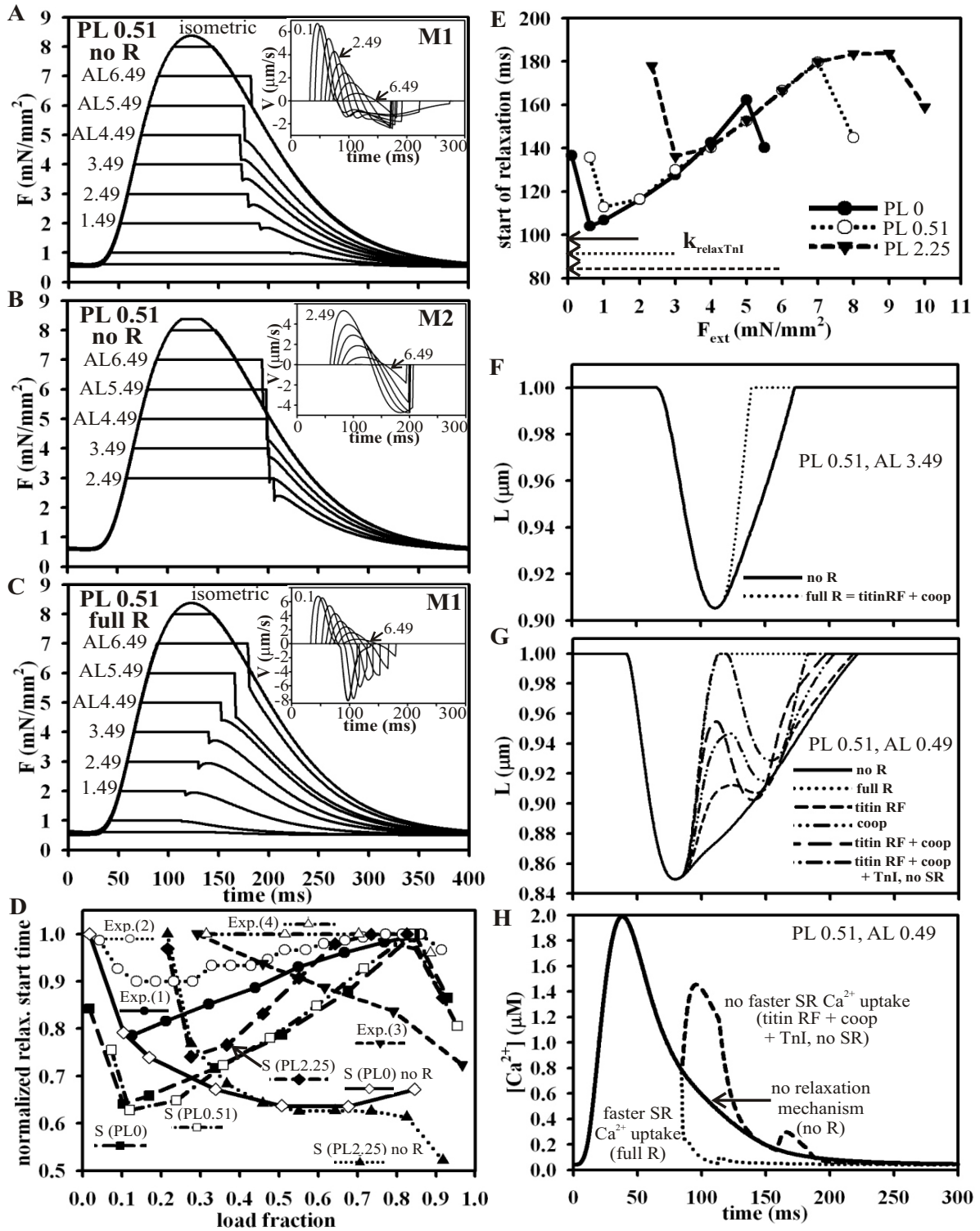


Fig. (10). Simulation analysis of shortening-induced deactivation and relaxation. The force time courses from afterloaded isotonic contraction for PL 0.51 are shown for M1 (A) and M2 (B) before adjustment of relaxation, i.e., without Eq. 48, Eq. 49, Eq. 51 and for M1 after adjustment of relaxation (C). The inserts in A, B and C depict the velocity time courses. Shortening-induced deactivation is absent in M2 (B). Panel D depicts the onset of the isometric relaxation of afterloaded isotonic contractions, which was measured from the start of the stimulation and normalized to the maximum of a data set, plotted against the load fraction for the following experimental data (Exp.) and simulations (S): Exp. (1), cat cardiac muscle, 29°C [51]; Exp. (2), cat cardiac muscle, 26°C [30]; Exp. (3), rat cardiac muscle, 29°C [51]; Exp. (4), rat cardiac muscle, 30°C [52]; S (PL 0), S (PL 0.51) and S (PL 2.25), simulation with the PL model with full relaxation

Fig. (10). Contd....

(Eq. 48-52); S (PL 0) no R and S (PL 2.25) no R, simulation with the PL model without adjustment of relaxation. In panel E the start time of the isometric relaxation given in (ms) for the three PL models with full relaxation is plotted against F_{ext} . The arrows indicate for which loads the relaxation was influenced by $k_{relaxTnI}$ (Eq. 50 for PL 0, Eq. 51 for PL 0.51 and Eq. 52 for PL 2.25). Panel F exhibits the L time courses for PL 0.51/ AL 3.49 (higher load) for two PL 0.51 model variants: no R, no relaxation (M1 without Eq. 48, Eq. 49, Eq. 51 and Eq. 58) and full R, full relaxation (M1 with Eq. 48, Eq. 49, Eq. 51 and Eq. 58). At this load $k_{relaxTnI} = k_{relaxSR} = 1$ and therefore full R = titin RF + coop, i.e., relaxation is load independent. Panel G shows the L time courses for PL 0.51/ AL 0.49 (low load) obtained with different PL 0.51 model variants as follows: no R, no relaxation (M1 without Eq. 48, Eq. 49, Eq. 51 and Eq. 58); full R, full relaxation (M1 with Eq. 48, Eq. 49, Eq. 51 and Eq. 58); titin RF, M1 with Eq. 48, lacks Eq. 49, Eq. 51 and Eq. 58; coop, M1 with Eq. 49, lacks Eq. 48, Eq. 51 and Eq. 58; titin RF+coop, M1 with Eq. 48, Eq. 49, lacks Eq. 51 and Eq. 58; titin RF+coop+TnI, no SR, M1 with Eq. 48, Eq. 49 and Eq. 51, lacks Eq. 58. Panel H shows the Ca^{2+} transient from some model variants as described for panel G.

model used. Although mathematically simple, it is biologically one of the most advanced models. In addition to having

physiological defined states, which stands in contrast to many previous models including a recently published model [12], various mechanisms such as a potential Frank-Starling mechanism, which was lately supported by some experimental evidence [41], and different cooperativity mechanisms [14] are included. Six out of 15 rate parameters are dynamically changing with species concentrations, SL or load, representing a quite realistic biological situation, where key reactions are constantly regulated to maintain homeostasis as e.g., the metabolic homeostasis of the heart [42]. Moreover, the present model includes detailed thin filament activation and is the only model that considers the conformational change of TnI, which was found to be an important regulatory step [43]. Rather than presenting normalized simulation results, as generally done in published contraction models, biological relevant data are given. This biological model structure can support the discovery of unknown mechanisms. Furthermore, this is the first simulation study that analyzes afterloaded contractions for different PLs in a quantitative way. Suggested mechanisms and simulation results are discussed below in context of model assumptions and limitations and compared to experimental findings.

The Rate Limiting Step in Myocyte Shortening

Simulation results highly depend on the chosen values for rate parameters in addition to model structure, since this determines the rate limiting steps, and further rely on which steps are decided to be load, SL or cooperativity dependent. Experimental evidence suggests that the ADP release rate is load-dependent [44-47] rather than the P_i release [45]. But which step of the Xb cycle is rate limiting is still not clarified. Based on skeletal muscle experiments the ADP release rate was reported to be the limiting step [44,46,47]. In contrast, Hinken & McDonald [48] showed using skinned rat cardiac myocytes at 13°C, that addition of P_i decreased force, but increased loaded shortening velocity for loads greater than 10% of the isometric force. They concluded that the P_i release is the rate limiting step at medium to higher load. Accordingly, the rate limiting step may well be changing with load. But results may also depend on the temperature and on temperature dependencies of rate parameters. In the present study, the ADP release rate (k_5) was chosen for model adjustment because it was the rate limiting step in the Xb cycle under isometric conditions and therefore appropriate for a key regulatory step. The model could well be adjusted for the desired velocity and end-systolic SL for medium to high load solely with a load-dependent change of k_5 .

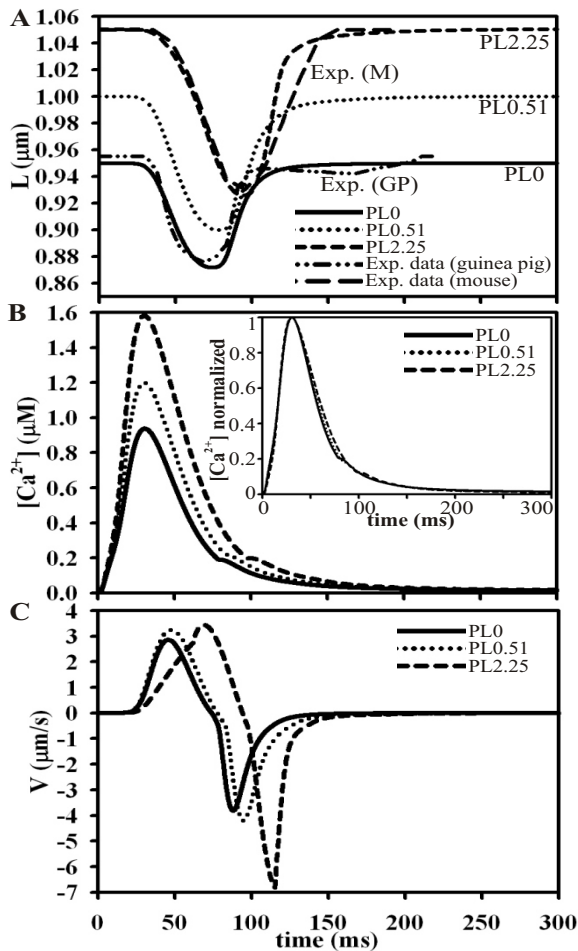


Fig. (11). Simulations of isotonic contractions with the Kyoto Model Ca^{2+} transient. In panel A simulation results for the L time courses for PL 0, 0.51 and 2.25 are compared to experimental data from a guinea pig left ventricular myocyte labeled as Exp. (GP) (37°C, slack length) [18] and a mouse right ventricular trabecula labeled as Exp. (M) (SL 2 to 2.1 µm, 37°C) [61]. The Ca^{2+} transients for the three PLs are shown in panel B. The peak of the Ca^{2+} transients were adjusted for the different PLs through a change of the Ca permeability of the L-type calcium channel (P_{CaL} of I_{CaL} in the Kyoto Model; Table 4, Eq. 19 in [16]) as follows: $P_{CaL}=4700$ for PL 0, 6000 for PL 0.51 and 8000 for PL 2.25. The insert shows the normalized Ca^{2+} transients. Panel C depicts the velocity time courses for the three different PLs.

The rise of k_5 is linear with an increase in velocity (Fig. 9B). At low load, however, the P_i release rate becomes rate limiting in the Xb cycle. A high velocity at low load could only be achieved with a high Xb turnover through an accelerated Tm conformational change mediated by the factor k_{loadTM} together with an increase in k_5 . At low to medium velocity k_{loadTM} is constant, but increases exponentially at high velocity (Fig. 9B). These rate parameter changes with velocity are comparable to experimental results from frog skeletal muscle [49]. A linear rise of the detachment rate with an increase in velocity was reported. The calculated apparent attachment rate under assumption of a two-state model was non-linearly increasing with velocity.

In the present model, the Tm conformational change rate at low load is the rate limiting step in the thin filament activation and its change was found to be most effective in obtaining a high velocity. So far this step has not been shown to be load or velocity dependent.

Regulation of Shortening- The [Xb] Determines the End-Systolic Sarcomere Length

Simulation data revealed that at medium to high load, which corresponds to a shortening velocity smaller than about 5 to 6 $\mu\text{m/s}$, the amount of shortening is determined by the peak [Xb], which decreases linearly with velocity (Fig. 9A). A small variation of the peak [Xb] is due to the fact that the Xb force is slightly velocity dependent (Fig. 8D and 8G). At low load, regardless of the PL, the peak [Xb] reaches the same almost constant value, and velocity is regulated by the thin filament activation speed (Fig. 9). Recently, X-ray interference and mechanical measurements performed with frog skeletal muscle fibers at 4°C revealed a linear decrease of attached Xbs with an increase in velocity [49]. Furthermore, these experiments showed that the force per attached Xb decreased with increasing velocity. But for small velocities these changes were small compared to the [Xb] change. From these data it was concluded that the FVR results from a decrease of the [Xb] with a fall in load [49]. Our simulation results coincide well with the above findings (Fig. 9). This is in contrast to previous suggestions, that the Xb force highly depends on load [6,7]. Comparing cardiac muscle simulation data with results from skeletal muscle experiments implies, however, that the chemomechanical transductions are at least similar between different myosins, an assumption that might be justified [47].

Although the present model contains a complex kinetics, the underlying mechanical principles are very simple. In particular, the ADP detachment rate depends on load, but is not directly influenced by the movement and strain of the Xb. Thus, the model only shows how the value of the rate parameters need to be modified with load, but cannot predict how the change is controlled by Xbs. So far these mechanisms have not been revealed by experiments making assumptions unavoidable in modeling. Many models specifically focusing on the mechanics were developed [6,9,12]. Various models utilize a variation of the Huxley-type model [7] with the detachment rate depending on the distance between the actin binding site and the myosin equilibrium posi-

tion [6,12]. In a recent Huxley-type model by Negroni and Lascano (NL model) [12] two attached Xb states, named weak and power state, were postulated each having a different elongation and therefore force. As in the present model the same basic Xb mechanics equation (Eq. 32) was used in the NL model but with a different interpretation and values of the parameters. The Xb detachment in the present model is coupled with the ADP release, and the detachment rate parameter (k_5) is load-dependent. In contrast, in the NL model, which does not specify the P_i or ADP release steps, the detachment occurs from a weak state. The detachment rate parameter depends on SL and the elongation of the weak Xb state, which is velocity dependent. Whereas in the present study B (Eq. 32) was shown to represent a load-dependent myosin characteristic which determines the shortening velocity in phase 2 of force step experiments (Eq. 39; Fig. 3C), in the NL model B is a constant. However, the NL model fails to correctly reproduce phase 2 of force step experiments with a not realistic length of the myosin stroke (Fig. 8A in [12]). These Huxley-type models have in common that the Xb force is greatly reduced during shortening and the myosin stroke size depends on the shortening velocity. However, recent experimental data challenged that view [49]. The stroke size was reported to be more or less constant over a large velocity range. Only a small change of the Xb force was detected at small to medium velocities and the [Xb]-velocity relationship was linear. The present model with just a load-dependent ADP release rate and both strong Xb states having the same constant force successfully reproduced these findings (Fig. 9).

Adjustment of the isometric model for the maximum [Xb] was done for full activation, i.e., tetanic steady state at high $[\text{Ca}^{2+}]$ and maximum SL (2.2 μm) to match experimental data performed under similar conditions (see section 3.1. in [14]). However, the degree and speed of the thin filament activation had to be balanced with the time to peak isometric force. For isotonic contractions especially at higher load and smaller SL the obtained number of Xbs is lower than physiologically supposed. Although this needs to be improved in the future, it is not expected to influence the current conclusions.

Titin-based Radial Force Mediates Shortening-Induced Cooperative Deactivation

The giant titin molecule has been implicated in many functions, due to its length and different domains [34]. While titin has no direct role in the actin-myosin interactions during shortening, it exhibits various regulatory roles. Although still controversial [34], titin-based radial force may alter the inter-filament spacing in a SL-dependent manner. This mechanism was included in the present model and tested for isometric contractions in a previous study [14]. A steep FLR as observed for cardiac muscle could be achieved with a SL-dependent change of the myosin binding rate. A lack of this titin-based mechanism caused a typical skeletal muscle FLR in the isometric model [14]. In the isotonic model, already at medium load a steep shortening to small SLs was observed (Fig. 6A). Such SLs are not naturally found in the intact

heart [50]. In the model SL shortening results in a titin regulated increase of the lateral space between thin and thick filaments, which slows down strong Xb formation. A decrease in the [Xb] enhances the rate for the TnI conformational change to the "off" state, thereby deactivating thin filaments. This potential Frank-Starling mechanism [14] accounts in the model for the shortening-induced cooperative deactivation. With a decrease of AL from a high to medium value, the time isometric relaxation starts is decreased in the model with titin (M1, Fig. 10A), but not in the model without titin (M2, Fig. 10B). Such load dependence was reported for afterloaded isotonic contractions performed with cat and pig cardiac muscle, but found to be small for rat and was missing in frog [30,51]. Furthermore, a decrease of this effect with an increase in temperature was detected in rat myocardium [52]. These species differences were suggested to depend on the Ca^{2+} uptake by the SR [30,51]. However, as predicted here, they may be explained by the included Frank-Starling mechanism. A variation of the titin isoform ratio, which is known to be highly species and tissue dependent [53], results in a varying strength of titin-based radial force. This may cause the different load dependence. Experimental evidence that strong Xbs modulate shortening velocity was reported: Length steps performed with rat single skinned cardiac myocytes revealed a progressive slow down of the shortening velocity at submaximum $[\text{Ca}^{2+}]$, which could be reduced by addition of N-ethylmaleimide-conjugated myosin subfragment-1 acting as a strong Xb equivalent [54]. A full mechanism, as proposed here, has not been revealed before. However, sarcomere shortening, resulting in an increase in filament spacing and hence, in a decrease of Xb formation, was proposed as part of the shortening-induced cooperative deactivation mechanism, stated to be important for relaxation as "myofibrillar brake system" [15]. Our simulation results show that this mechanism is significant, but alone cannot account for a fast and complete relaxation, especially at lower load (Fig. 10A).

Fast Relaxation due to Enhanced Thin Filament Deactivation

An altered ventricular relaxation results in an impaired filling and therefore an inappropriate cardiac output. Since diastolic dysfunction is associated with various cardiomyopathies, elucidating the mechanisms underlying relaxation is of great importance [55]. Isotonic relaxation was shown to be faster than isotonic shortening [38]. Although various intrinsic and extrinsic mechanisms were found to play a role in the regulation [55], how cardiac muscle achieves these high relaxation velocities is not well understood. The fast early relaxation phase was recently attributed to titin restoring force [21] and could be explained as elastic recoil of the titin molecule [20]. However, how the release of the elastic energy from each single titin molecule speeds up relaxation is unknown. Experiments show no change of the interfilament lattice spacing, but a conformational disorder was suggested around the start of relaxation since a buckling of myosin filaments was observed [21]. Here, it was assumed that the detected disorder might be a disruption of the Tm filament structure leading to a SL-dependent increase in the Tm

conformational change rate to the "off" state (k_{tmoff}) during relaxation. A variation of k_{tmoff} greatly affected relaxation speed, whereas a variation of Xb cycle rate parameters such as an increase in k_{-12} , k_{-3} , k_{-4} or k_5 had only a minor effect. While an increase in $[\text{P}_i]$ was reported to speed up relaxation [56], in the model a faster P_i addition did not improve relaxation. Moreover, an increase in the transition from strong Xbs to pre-power states during stretch was suggested to save chemical energy and enhance relaxation [56]. The question remains what prevents these pre-power states from reattachment. This of course occurs in the present model preventing a fast relaxation. Overall in the model the effect from titin restoring force was rather small (Fig. 10G) suggesting that this is not a major relaxation mechanism.

A structural study revealed that TnI in the "off" conformation pulls Tm to the "off" conformation [35]. This mechanism was further supported by an electron microscopy study that showed that at a low $[\text{Ca}^{2+}]$ the C-terminal TnI domain competes with Tm for a common actin binding site, thus pushing Tm into the blocking position [57]. Recently, the TnI Lys184 deletion, which is located in the C-terminal mobile domain and linked to familial hypertrophic cardiomyopathy, which is associated with diastolic dysfunction, was reported to slow down relaxation in mouse left-ventricular papillary muscle fibers and to increase thin filament Ca^{2+} sensitivity [58]. In our model a feedback of $[\text{RUTCaoff}]$ on k_{tmoff} strongly speeded up early relaxation (Fig. 10G). This mechanism together with the titin restoring force was sufficient for a fast relaxation velocity at medium to high load (Fig. 10E and 10F).

With decreasing load, late relaxation was slowed, especially at higher PLs (Fig. 10E-G), but could be improved through a load-dependent increase in the TnI conformational change rate to the "off" state (k_{off}). An increase of k_{off} during relaxation might play an important role in the extrinsic regulation of cardiac output. TnI phosphorylation by protein kinase A during β -adrenergic stimulation weakens the TnC Ca^{2+} affinity and enhances relaxation [59]. Furthermore, experiments showed an increase in TnI phosphorylation with an increase in AL [60].

CONCLUSION

The development of a unique cardiac muscle contraction model that includes detailed thin filament activation is described here. Xb mechanics was adjusted through simulations of P1 and P2 of force steps. Adjustment of the Xb kinetics was achieved through simulations of afterloaded isotonic contractions, while considering that for different PLs but the same total load, the same end-systolic SL is reached. Simulation results show that in the load range relevant to the intact heart the end-systolic SL was mainly determined by the [Xb], while the [Xb] was regulated by the load-dependent ADP release rate. Instead, the change of the Xb force with a change in the shortening velocity was small. Shortening-induced cooperative deactivation was attributed to the included Frank-Starling mechanism. For a good relaxation the speed of the thin filament deactivation was more significant than the Xb detachment rate. A fast relaxation

was achieved mainly through an increased rate of the Tm conformational change to the “off” state.

In the future, this model will need to be tested for its energetic performance and for auxotonic contractions in a circulation model to mimic the intact heart conditions with PL and AL constantly changing. Due to its biological realism the model, which can be easily inserted into any myocyte or circulation model, will allow for significantly more realistic physiological and pathophysiological cardiac muscle contraction studies than previously available models.

ACKNOWLEDGEMENTS

The authors wish to thank Prof. Matsuoka for suggestions to improve this manuscript. The first author expresses her gratitude to Prof. Mitsuiye for providing an office space. This study was supported by the Leading Project for Biosimulation from the Ministry of Education, Culture, Sports, Science and Technology of Japan.

ABBREVIATIONS

AL	=	Afterload
FVR	=	Force-velocity relationship
L_{\min}	=	End-systolic L
LTR	=	Length-tension relationship
MHC	=	Myosin heavy chain
P1	=	Phase 1
P2	=	Phase 2
PL	=	Preload
RU	=	Regulatory unit
SL	=	Sarcomere length
SR	=	Sarcoplasmic reticulum
Tm	=	Tropomyosin
Tn	=	Troponin
TnC	=	Troponin C
TnI	=	Troponin I
TnT	=	Troponin T
Xb	=	Cross-bridge
[Xb]	=	Cross-bridge concentration

APPENDIX

Glossary

A:	actin
α :	sarcomere overlap function
A_f :	force factor
B:	proportionality factor; contains myosin isoform characteristic
F_b :	active force
F_{ext} :	external force (load)

F_p : passive force

$F_{p\text{Ex}}$: F_p contribution from collagen

$F_{p\text{IF}}$: F_p contribution from intermediate filaments

$F_{p\text{Titin}}$: F_p contribution from titin

h: Xb elongation

h_c : steady state Xb elongation

k_{12} : myosin binding rate parameter

k_{-12} : myosin detachment rate parameter

k_3 : rate parameter for the strong Xb formation

k_{-3} : rate parameter for the transition from the strong to the weak Xb

k_{3c} : factor for k_3 , k_{-3} at resting level

k_{3f} : factor determining the positive cooperativity caused by neighboring activated RUs affecting the strong Xb formation

k_{3b} : factor for negative cooperativity caused by strong Xbs affecting the strong Xb formation

k_{-4} : P_i binding rate parameter

k_4 : P_i release rate parameter

k_5 : ADP release rate parameter

k_{loadTM} : factor expressing the load dependence for the Tm conformational change to the “on” conformation at low load shortening

K_m : SR pump parameter

k_{off} : Ca^{2+} detachment rate constant

k_{OFF} : factor for the positive cooperativity caused by neighboring RUs in the activated conformation

k_{off} : factor for k_{offI} , k_{offII} at resting level

k_{offI} : rate for the TnI conformational change to the “off” conformation

k_{offrelax} : factor for k_{offTnI}

k_{offTnI} : factor for cooperativity caused by TnI in the “off” conformation pulling Tm to the “off” conformation

k_{on} : Ca^{2+} binding rate constant

k_{onI} : rate for the TnI conformational change to the “on” conformation

K_p : maximum value of Q_{pump}

k_{relaxSR} : factor to enhance Ca^{2+} uptake during relaxation

k_{relaxTnI} : factor for enhancing the TnI conformational change to the “off” conformation

k_{Titin} : scaling factor for the titin function

K_{Titin} : titin function

k_{tmonoff} : rate parameter for the Tm conformational change to the “off” conformation

k_{tmonon} : rate parameter for the Tm conformational change to the “on” conformation

k_{tmonc} : factor for k_{tmon} , k_{tmon} at resting level

k_{tmRU} : factor determining the positive cooperativity caused by neighboring activated RUs affecting the Tm conformational change to the “on” conformation

k_{tmxb} : factor for negative cooperativity caused by strong Xbs affecting the Tm conformational change to the “on” conformation

k_{xboff} : factor for the positive cooperativity caused by strong Xbs

L: half sarcomere length

L_0 : normalization factor

L_1 : length change due to muscle elasticity in force step P1

L_2 : sum of L_1 plus L_T

L_T : myosin working stroke, length change in P2

load: load fraction

M: myosin

Q_{ADPR} : net rate of the ADP release step

Q_{CaB} : net rate for Ca^{2+} binding to TnC

Q_{Fgen} : net rate of the force generating step

Q_m : maximum Q_{rel} value

Q_{MB} : net rate of the myosin binding step

Q_{PiR} : net rate of the P_i release step

Q_{pump} : SR Ca^{2+} uptake net rate

Q_{pumprest} : Q_{pump} under resting conditions

Q_{rel} : Ca^{2+} release from the SR

Q_{TcaA} : net rate for the TnI conformational change

Q_{TMA} : net rate of the Tm conformational change

RU: regulatory unit

RUA: activated RUs

RUA_MADP: strong Xb, P_i released from the acto-myosin complex

RUA_MADPPi: strong Xb, M pocket for P_i open

RUAMADPPi: M with a hydrolyzed ATP bound to A of a activated RU (weak Xb); M pocket for P_i closed

RUNA: not activated RU

RUTCaoff: Ca^{2+} bound to TnC with TnI still bound to A

RUTCaon: TnI released from A

RUTMon: Tm in the activated conformation

RUtotal: sum of all RUs

t: time

t_1 : time to Q_m

t_2 : force step phase 2 time interval

titinRF: factor expressing the effect from titin restoring force during relaxation

Tm: tropomyosin

TnC: troponin C

TnI: troponin I

V2: force step phase 2 shortening velocity

X: part of L which is not covered by h

REFERENCES

- [1] Norton JM. Toward consistent definitions for preload and afterload. *Adv Physiol Educ* 2001; 25: 53-61.
- [2] Sonnenblick EH, Parmley WW, Urschel CW. The contractile state of the heart as expressed by force-velocity relations. *Am J Cardiol* 1969; 23: 488-503.
- [3] Brutsaert DL, Sonnenblick EH. Force-velocity-length-time relations of the contractile elements in heart muscle of the cat. *Circ Res* 1969; 24: 137-49.
- [4] de Tombe PP, ter Keurs HE. Sarcomere dynamics in cat cardiac trabeculae. *Circ Res* 1991; 68: 588-96.
- [5] Piazzesi G, Lucii L, Lombardi V. The size and the speed of the working stroke of muscle myosin and its dependence on the force. *J Physiol* 2002; 545: 145-51.
- [6] Edman KA, Mansson A, Caputo C. The biphasic force-velocity relationship in frog muscle fibres and its evaluation in terms of cross-bridge function. *J Physiol* 1997; 503: 141-56.
- [7] Huxley AF. Muscle structure and theories of contraction. *Prog Biophys Biophys Chem* 1957; 7: 255-318.
- [8] Duke TA. Molecular model of muscle contraction. *Proc Natl Acad Sci U S A* 1999; 96: 2770-5.
- [9] Lan G, Sun SX. Dynamics of myosin-driven skeletal muscle contraction: I. Steady-state force generation. *Biophys J* 2005; 88: 4107-17.
- [10] Chin L, Yue P, Feng JJ, Seow CY. Mathematical simulation of muscle cross-bridge cycle and force-velocity relationship. *Biophys J* 2006; 91: 3653-63.
- [11] Negroni JA, Lascano EC. A cardiac muscle model relating sarcomere dynamics to calcium kinetics. *J Mol Cell Cardiol* 1996; 28: 915-29.
- [12] Negroni JA, Lascano EC. Simulation of steady state and transient cardiac muscle response experiments with a Huxley-based contraction model. *J Mol Cell Cardiol* 2008; 45: 300-12.
- [13] Rice JJ, Wang F, Bers DM, de Tombe PP. Approximate model of cooperative activation and crossbridge cycling in cardiac muscle using ordinary differential equations. *Biophys J* 2008; 95: 2368-90.
- [14] Schneider NS, Shimayoshi T, Amano A, Matsuda T. Mechanism of the Frank-Starling law--a simulation study with a novel cardiac muscle contraction model that includes titin and troponin I. *J Mol Cell Cardiol* 2006; 41: 522-36.
- [15] Hanft LM, Korte FS, McDonald KS. Cardiac function and modulation of sarcomeric function by length. *Cardiovasc Res* 2008; 77: 627-36.
- [16] Matsuoka S, Sarai N, Kuratomi S, Ono K, Noma A. Role of individual ionic current systems in ventricular cells hypothesized by a model study. *Jpn J Physiol* 2003; 53: 105-23.
- [17] Gordon AM, Homsher E, Regnier M. Regulation of contraction in striated muscle. *Physiol Rev* 2000; 80: 853-924.
- [18] Sasaki N, Mitsuiye T, Noma A, Powell T. Sarcomere length during contraction of isolated guinea-pig ventricular myocytes. *Pflugers Arch* 1999; 437: 804-11.
- [19] Granzier HL, Irving TC. Passive tension in cardiac muscle: contribution of collagen, titin, microtubules, and intermediate filaments. *Biophys J* 1995; 68: 1027-44.
- [20] Nair P, Wu Y, Helmes M, *et al.* Restoring force development by titin/connectin and assessment of Ig domain unfolding. *J Muscle Res Cell Motil* 2005; 26: 307-17.
- [21] Helmes M, Lim CC, Liao R, *et al.* Titin determines the Frank-Starling relation in early diastole. *J Gen Physiol* 2003; 121: 97-110.
- [22] Reconditi M, Linari M, Lucii L, *et al.* Structure-function relation of the myosin motor in striated muscle. *Ann N Y Acad Sci* 2005; 1047: 232-47.
- [23] Linari M, Brunello E, Reconditi M, *et al.* The structural basis of the increase in isometric force production with temperature in frog skeletal muscle. *J Physiol* 2005; 567: 459-69.

- [24] Decostre V, Bianco P, Lombardi V, Piazzesi G. Effect of temperature on the working stroke of muscle myosin. *Proc Natl Acad Sci USA* 2005; 102: 13927-32.
- [25] Mathur AB, Collinsworth AM, Reichert WM, Kraus WE, Truskey GA. Endothelial, cardiac muscle and skeletal muscle exhibit different viscous and elastic properties as determined by atomic force microscopy. *J Biomech* 2001; 34: 1545-53.
- [26] Colombini B, Nocella M, Benelli G, Cecchi G, Bagni MA. Effect of temperature on cross-bridge properties in intact frog muscle fibers. *Am J Physiol* 2008; 294: C1113-7.
- [27] Piazzesi G, Reconditi M, Koubassova N, *et al.* Temperature dependence of the force-generating process in single fibres from frog skeletal muscle. *J Physiol* 2003; 549: 93-106.
- [28] Sieck GC, Regnier M. Invited review: plasticity and energetic demands of contraction in skeletal and cardiac muscle. *J Appl Physiol* 2001; 90: 1158-64.
- [29] Hinken AC, McDonald KS. Beta-myosin heavy chain myocytes are more resistant to changes in power output induced by ischemic conditions. *Am J Physiol* 2006; 290: H869-77.
- [30] Donald TC, Reeves DN, Reeves RC, Walker AA, Hefner LL. Effect of damaged ends in papillary muscle preparations. *Am J Physiol* 1980; 238: H14-23.
- [31] Brutsaert DL, Sonnenblick EH. Cardiac muscle mechanics in the evaluation of myocardial contractility and pump function: problems, concepts, and directions. *Prog Cardiovasc Dis* 1973; 16: 337-61.
- [32] Iribe G, Helmes M, Kohl P. Force-length relations in isolated intact cardiomyocytes subjected to dynamic changes in mechanical load. *Am J Physiol* 2007; 292: H1487-97.
- [33] Sonnenblick EH, Skelton CL. Reconsideration of the ultrastructural basis of cardiac length-tension relations. *Circ Res* 1974; 35: 517-26.
- [34] Fukuda N, Granzier HL, Ishiwata S, Kurihara S. Physiological functions of the giant elastic protein titin in Mammalian striated muscle. *J Physiol Sci* 2008; 58: 151-9.
- [35] Murakami K, Yumoto F, Ohki SY, *et al.* Structural basis for Ca²⁺-regulated muscle relaxation at interaction sites of troponin with actin and tropomyosin. *J Mol Biol* 2005; 352: 178-201.
- [36] Sarai N, Matsuoka S, Noma A. simBio: a Java package for the development of detailed cell models. *Prog Biophys Mol Biol* 2006; 90: 360-77.
- [37] Press WH, Flannery BP, Teukolsky SA, Vetterling WT. Numerical recipes in C: the art of scientific computing. 2nd ed. Cambridge University Press: Cambridge 1992.
- [38] Brutsaert DL, Sys SU. Relaxation and diastole of the heart. *Physiol Rev* 1989; 69: 1228-315.
- [39] Monasky MM, Varian KD, Davis JP, Janssen PM. Dissociation of force decline from calcium decline by preload in isolated rabbit myocardium. *Pflugers Arch* 2008; 456: 267-76.
- [40] Wan X, Bryant SM, Hart G. A topographical study of mechanical and electrical properties of single myocytes isolated from normal guinea-pig ventricular muscle. *J Anat* 2003; 202: 525-36.
- [41] Terui T, Sodnomtseren M, Matsuba D, *et al.* Troponin and titin coordinately regulate length-dependent activation in skinned porcine ventricular muscle. *J Gen Physiol* 2008; 131: 275-83.
- [42] Balaban RS. Maintenance of the metabolic homeostasis of the heart: developing a systems analysis approach. *Ann N Y Acad Sci* 2006; 1080: 140-53.
- [43] Robinson JM, Dong WJ, Xing J, Cheung HC. Switching of troponin I: Ca(2+) and myosin-induced activation of heart muscle. *J Mol Biol* 2004; 340: 295-305.
- [44] Nyitrai M, Geeves MA. Adenosine diphosphate and strain sensitivity in myosin motors. *Philos Trans R Soc Lond B Biol Sci* 2004; 359: 1867-77.
- [45] Sleep J, Irving M, Burton K. The ATP hydrolysis and phosphate release steps control the time course of force development in rabbit skeletal muscle. *J Physiol* 2005; 563: 671-87.
- [46] Guo B, Guilford WH. Mechanics of actomyosin bonds in different nucleotide states are tuned to muscle contraction. *Proc Natl Acad Sci U S A* 2006; 103: 9844-9.
- [47] Capitanio M, Canepari M, Cacciafesta P, *et al.* Two independent mechanical events in the interaction cycle of skeletal muscle myosin with actin. *Proc Natl Acad Sci U S A* 2006; 103: 87-92.
- [48] Hinken AC, McDonald KS. Inorganic phosphate speeds loaded shortening in rat skinned cardiac myocytes. *Am J Physiol* 2004; 287: C500-7.
- [49] Piazzesi G, Reconditi M, Linari M, *et al.* Skeletal muscle performance determined by modulation of number of myosin motors rather than motor force or stroke size. *Cell* 2007; 131: 784-95.
- [50] Burkholder TJ, Lieber RL. Sarcomere length operating range of vertebrate muscles during movement. *J Exp Biol* 2001; 204: 1529-36.
- [51] Brutsaert DL, de Clerck NM, Goethals MA, Housmans PR. Relaxation of ventricular cardiac muscle. *J Physiol* 1978; 283: 469-80.
- [52] Dobrunz LE, Berman MR. Effect of temperature on Ca⁽²⁺⁾-dependent and mechanical modulators of relaxation in mammalian myocardium. *J Mol Cell Cardiol* 1994; 26: 243-50.
- [53] Neagoe C, Opitz CA, Makarenko I, Linke WA. Gigantic variety: expression patterns of titin isoforms in striated muscles and consequences for myofibrillar passive stiffness. *J Muscle Res Cell Motil* 2003; 24: 175-89.
- [54] McDonald KS, Moss RL. Strongly binding myosin crossbridges regulate loaded shortening and power output in cardiac myocytes. *Circ Res* 2000; 87: 768-73.
- [55] Borlaug BA, Kass DA. Mechanisms of diastolic dysfunction in heart failure. *Trends Cardiovasc Med* 2006; 16: 273-9.
- [56] Poggesi C, Tesi C, Stehle R. Sarcomeric determinants of striated muscle relaxation kinetics. *Pflugers Arch* 2005; 449: 505-17.
- [57] Galinska-Rakoczy A, Engel P, Xu C, *et al.* Structural basis for the regulation of muscle contraction by troponin and tropomyosin. *J Mol Biol* 2008; 379: 929-35.
- [58] Iorga B, Blaudeck N, Solzin J, *et al.* Lys184 deletion in troponin I impairs relaxation kinetics and induces hypercontractility in murine cardiac myofibrils. *Cardiovasc Res* 2008; 77: 676-86.
- [59] Solaro RJ, Rosevear P, Kobayashi T. The unique functions of cardiac troponin I in the control of cardiac muscle contraction and relaxation. *Biochem Biophys Res Commun* 2008; 369: 82-7.
- [60] Takimoto E, Soergel DG, Janssen PM, *et al.* Frequency- and afterload-dependent cardiac modulation *in vivo* by troponin I with constitutively active protein kinase A phosphorylation sites. *Circ Res* 2004; 94: 496-504.
- [61] Stuyvers BD, McCulloch AD, Guo J, Duff HJ, ter Keurs HE. Effect of stimulation rate, sarcomere length and Ca(2+) on force generation by mouse cardiac muscle. *J Physiol* 2002; 544: 817-30.
- [62] Robinson JM, Wang Y, Kerrick WG, Kawai R, Cheung HC. Activation of striated muscle: nearest-neighbor regulatory-unit and cross-bridge influence on myofilament kinetics. *J Mol Biol* 2002; 322: 1065-88.
- [63] Sachse FB, Glänzel KG, Seemann G. Modeling of protein interactions involved in cardiac tension development. *Int J Bifurcat Chaos* 2003; 13: 3561-78.
- [64] Gordon AM, Regnier M, Homsher E. Skeletal and cardiac muscle contractile activation: tropomyosin "rocks and rolls". *News Physiol Sci* 2001; 16: 49-55.

Received: November 03, 2008

Revised: May 05, 2009

Accepted: May 31, 2009

© Schneider and Amano; Licensee Bentham Open.

This is an open access article licensed under the terms of the Creative Commons Attribution Non-Commercial License (<http://creativecommons.org/licenses/by-nc/3.0/>) which permits unrestricted, non-commercial use, distribution and reproduction in any medium, provided the work is properly cited.